CrossMark

RADIO AND SPACE-BASED OBSERVATIONS

A Statistical Analysis of the Solar Phenomena Associated with Global EUV Waves

D.M. Long [1] · **P. Murphy**[2] · **G. Graham**[1] ·
E.P. Carley[2] · **D. Pérez-Suárez**[1]

Abstract Solar eruptions are the most spectacular events in our solar system and are associated with many different signatures of energy release including solar flares, coronal mass ejections, global waves, radio emission and accelerated particles. Here, we apply the Coronal Pulse Identification and Tracking Algorithm (CorPITA) to the high-cadence synoptic data provided by the *Solar Dynamics Observatory* (SDO) to identify and track global waves observed by SDO. 164 of the 362 solar flare events studied (45%) were found to have associated global waves with no waves found for the remaining 198 (55%). A clear linear relationship was found between the median initial velocity and the acceleration of the waves, with faster waves exhibiting a stronger deceleration (consistent with previous results). No clear relationship was found between global waves and type II radio bursts, electrons or protons detected *in situ* near Earth. While no relationship was found between the wave properties and the associated flare size (with waves produced by flares from B to X-class), more than a quarter of the active regions studied were found to produce more than one wave event. These results suggest that the presence of a global wave in a solar eruption is most likely determined by the structure and connectivity of the erupting active region and the surrounding quiet solar corona rather than by the amount of free energy available within the active region.

✉ D.M. Long
david.long@ucl.ac.uk

1   UCL-Mullard Space Science Laboratory, Holmbury St. Mary, Dorking, Surrey, RH5 6NT, UK

2   School of Physics, Trinity College Dublin, College Green, Dublin 2, Ireland

 Springer

1. Introduction

Global waves in the low solar corona (commonly called "EIT waves") were first observed using the *Extreme ultraviolet Imaging Telescope* (EIT; Delaboudinière *et al.*, 1995) on board the *Solar and Heliospheric Observatory* (SOHO; Domingo, Fleck, and Poland, 1995). Initially identified as fast-mode MHD waves (*e.g.* Dere *et al.*, 1997; Moses *et al.*, 1997; Thompson *et al.*, 1998), this interpretation was questioned following observations of stationary bright fronts at coronal hole boundaries and anomalously low measured kinematics (*cf.* Delannée and Aulanier, 1999). This led to the development of two distinct families of theories to describe this phenomenon; that they are alternatively waves (either linear or non-linear waves) or pseudo-waves (*i.e.* a brightening resulting from the restructuring of the coronal magnetic field during the eruption of a coronal mass ejection). Note that a more detailed overview of the different theories proposed to explain the "EIT wave" phenomenon may be found in the recent reviews by Liu and Ofman (2014) and Warmuth (2015). However, the advent of high-cadence observations with the launch of the *Solar Terrestrial Relations Observatory* (STEREO; Kaiser *et al.*, 2008) and *Solar Dynamics Observatory* (SDO; Pesnell, Thompson, and Chamberlin, 2012) spacecraft has begun to refine our understanding of this phenomenon. Recent work comparing the predictions made by each of these theories with observations suggests that they are best described as large-amplitude waves initially driven by the rapid lateral expansion of a CME in the low corona, before propagating freely (*cf.* Long *et al.*, 2017).

Although our understanding of the origin and physical properties of global waves has progressed since they were first observed, their relationship with other solar phenomena such as solar flares, CMEs, solar energetic particles (SEPs) and radio bursts continues to be a source of investigation. Global EIT waves have traditionally been studied using single event case studies, making it difficult to draw general conclusions about the nature of their relationship with these phenomena. Recognising this issue, a catalogue of global EIT waves observed by SOHO/EIT was assembled by Thompson and Myers (2009), with each wave event identified "by eye" and classified using a quality rating system. This catalogue was subsequently used to investigate the link between global EIT waves and other solar phenomena including type II radio bursts, solar flares and CMEs (*e.g.* Biesecker *et al.*, 2002; Warmuth and Mann, 2011). More recent work has extended this systematic approach to observations from the *Extreme UltraViolet Imager* (EUVI; Wuelser *et al.*, 2004) on board STEREO (Muhr *et al.*, 2014; Nitta *et al.*, 2014) and SDO/AIA (Nitta *et al.*, 2013). In each of these cases the global waves were identified using semi-automated techniques; Muhr *et al.* (2014) defined the direction into which the wavefront propagated and used a perturbation profile technique to fit the leading edge of the wavefront while Nitta *et al.* (2013, 2014) used 2D intensity stack plots produced by a series of arc sectors to visually identify the leading edge of the wavefront. Each approach requires manual input from the user, potentially making them susceptible to user bias. In addition, the catalogues created using observations from SOHO/EIT and STEREO/EUVI may have been subject to the lower temporal resolution of both instruments, which could have led to a systematic under-estimation of the kinematics of the global waves (*cf.* Byrne *et al.*, 2013).

Despite these issues, the catalogues developed by Thompson and Myers (2009) (in particular), Muhr *et al.* (2014) and Nitta *et al.* (2013) have been widely used to study the relationship between global waves and other solar phenomena such as type II radio bursts, solar flares and CMEs. Although initially ambiguous, the relationship between global waves and CMEs is now well defined, with Biesecker *et al.* (2002) showing that every wave has an associated CME, although not every CME has an associated wave. Type II radio bursts have long

been observed in the solar corona associated with solar eruptions (*e.g.* Payne-Scott, Yabsley, and Bolton, 1947; Wild and McCready, 1950) and it was generally accepted that both type II bursts and Moreton–Ramsey waves (first observed in the 1960s by Moreton, 1960; Moreton and Ramsey, 1960) were signatures of the same driving process (Uchida, 1968). However, the much lower measured speeds and other discrepancies between Moreton–Ramsey and global EIT waves complicated extending this assumption to EIT waves. Instead, Klassen *et al.* (2000) found that 90% of type II bursts identified in 1997 were associated with EIT waves. In contrast, Biesecker *et al.* (2002) used the wave event list compiled by Thompson and Myers (2009) to show that only 29% of the waves in the list had an associated type II radio burst. This percentage was supported by an analysis of 60 global EUV waves observed by STEREO/EUVI and studied by Muhr *et al.* (2014), who found that 22% of the global waves studied had an associated type II radio burst. However, a study of 138 global waves identified by Nitta *et al.* (2013) using SDO/AIA found that 54% of the waves were associated with a type II radio burst. The exact nature of the connection between global waves and type II radio bursts therefore remains subject to investigation.

The energy release during a solar eruption (either as a flare or through acceleration of a CME) can also result in solar energetic particles (SEPs) being accelerated into the heliosphere. SEPs are known to fall into two general categories, impulsive (typically associated with particle acceleration in a small area such as a solar flare) and gradual (associated with particle acceleration over a broad area, such as from a CME) as described by Reames (1993). Release of gradual SEPs tends to occur close to the Sun, where the CME shocks as it propagates outwards into the heliosphere (*e.g.* Kahler, 1994). This process can also occur in the low corona, with the lateral expansion of the CME shock front accelerating SEPs (*e.g.* Rouillard *et al.*, 2012) as it propagates through the low corona. The result of this impulsive lateral expansion is best observed as a global EUV wave (*cf.* Long *et al.*, 2017). Despite this, there is no clear relationship between global EUV waves and SEP events, with most previous work tending to focus on individual case-study events (*e.g.* Kozarev *et al.*, 2011; Prise *et al.*, 2014). The measured SEP detection time is then typically used to infer the time and location that the particles (both protons and electrons) were released on the Sun, which can be compared to the tracked evolution of the global wave in the low corona (*e.g.* Rouillard *et al.*, 2012; Prise *et al.*, 2014). This approach was also used by Miteva *et al.* (2014) to study 179 SEP events between 1997 and 2006, finding that protons detected *in situ* were related to the global EUV waves, but that there was no correlation between the waves and electrons.

Here we describe the application of an automated algorithm to observations from SDO/AIA to identify and characterise global EUV waves and relate them to other solar phenomena such as flares, CMEs, SEP events and type II radio bursts. The various data-sets and how the measurements were made are described in Section 2, with the results of the statistical analysis described in Section 3. The results are then discussed and some conclusions drawn in Section 4. Note that the complete table used for the analysis described here is also included in the Appendix.

2. Observations and Data Analysis

The list of global EUV waves identified by Nitta *et al.* (2013) was used as a starting point for this investigation to maximise the number of global wave events and associated phenomena that could be studied in detail. In each case, the location of the flare associated with each eruption was used as the source of the global wave, with the start time of the flare used as the reference point for analysing the EUV, radio and *in situ* data.
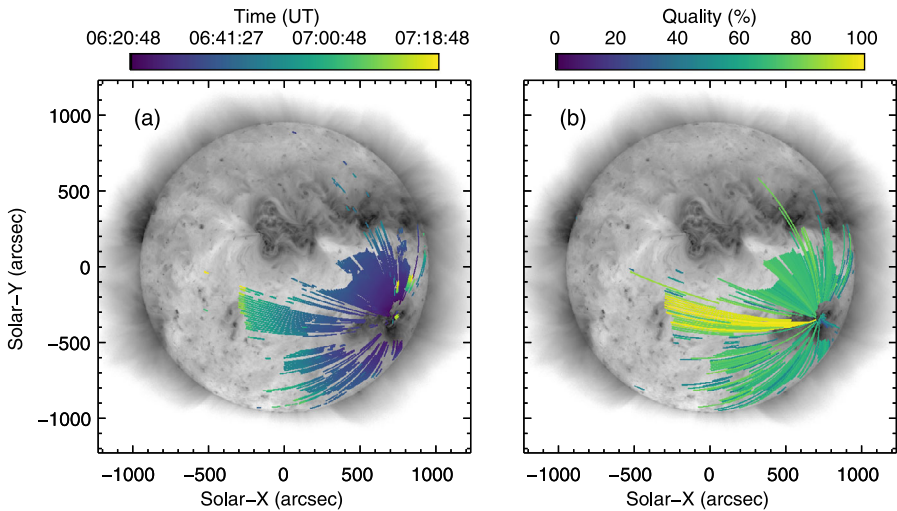
Figure 1 Panel **a** Temporal evolution of the global wave associated with the solar eruption on 7 June 2011 derived using the CorPITA code with colour showing time since 06:20:48 UT. Panel **b** The quality rating (*cf.* Long *et al.*, 2014) associated with each arc sector.

2.1. Global Wave Characterisation and Analysis

The events listed in the wave list of Nitta *et al.* (2013) were processed using the Coronal Pulse Identification and Tracking Algorithm (CorPITA; Long *et al.*, 2014). CorPITA is an automated code designed to identify, track and analyse global EUV waves using science quality data from the SDO/AIA 211 Å passband. Although global waves have previously been characterised using each of the eight extreme ultraviolet (EUV) passbands observed by SDO (Liu *et al.*, 2011), previous work has shown that they are best observed using either the 193 Å or 211 Å passbands (Long *et al.*, 2014). The 211 Å passband was used here as it observes slightly hotter plasma than the 193 Å passband and as a result does not have as much emission from the background corona, making the global wave easier to identify and characterise.

Percentage base-difference images are used to identify the wave pulse, with the pre-event image defined as the image 2 minutes prior to the start time of the flare. A series of 360 arc sectors, each of 10° wide and offset by 1°, centered on the flare location are then used to define a series of intensity profiles. The wave pulse is identified using these intensity profiles and fitted using a Gaussian function which allows the position (*i.e.* the centroid of the Gaussian), peak intensity and full-width at half-maximum to be recorded in each arc sector for each time step. The CorPITA code then identifies the pulse in each arc sector by finding the largest section of contiguous data-points exhibiting increasing distance away from the source point. This section of data-points is then fitted using a quadratic function which provides an estimate of the initial pulse velocity and acceleration. The temporal variation in pulse distance from the source point for the 7 June 2011 event is shown in Figure 1a. Although this technique ensures a consistent approach to estimating the initial pulse velocity and acceleration of the pulse, the accuracy can be affected by sudden jumps in pulse position (*e.g.* due to the algorithm becoming confused by bright points or small-scale loop oscillations). The accuracy of the measurement in each arc sector is therefore quantified in each case using a quality rating system, with the pulse scored according to the number of

images used to identify it, the fitted initial velocity and acceleration and the uncertainty in identifying the pulse (*cf.* Long *et al.*, 2014). Figure 1b shows the estimated quality rating for each of the arc sectors studied for the 7 June 2011 event. A wave is then identified by CorPITA if more than 10 adjacent arc sectors detect a moving pulse with a quality rating greater than 60%. The measured parameters of the wave identified by CorPITA are then stored for future use (as listed in Table 1). In addition to the location of the source, start time of the wave and fitted kinematics, CorPITA also records the number of arcs in the largest segment in which CorPITA has identified a wave (corresponding to the column Num. arcs in Table 1) and the central arc of this segment in degrees clockwise from solar north (Central arc angle). Note that Central arc angle uses the central angle of the segment to indicate the mean direction of the identified wave pulse, and does not necessarily correspond to the highest rated arc within that segment.

Although a more detailed description of the CorPITA technique may be found in the paper by Long *et al.* (2014), it should be noted that the code has since been updated to address issues found during an initial attempt at the work described here. Data is now downloaded in 20 minute chunks to speed up processing rather than an initial 10 minute chunk followed by single image downloading as before. This increase in time over which to search for a wave provides a better opportunity to identify the wave pulse, particularly for gradual flare events where the starting time of the wave and starting time of the flare may not be well correlated. The code has been rewritten for stability and to ensure a more rigorous analysis, while the colour table has also been updated to make it more accessible and easier to understand (as shown in Figure 1).

2.2. Solar Energetic Particle Analysis

The SEP events associated with each global wave event were identified using measurements from the 3D EESA/PESA (Lin *et al.*, 1995) instrument on board the *Wind* spacecraft. The data for electrons of energies between ≈ 1.3 keV and ≈ 27 keV and protons of energies between ≈ 195 keV and ≈ 4.4 MeV were examined for 24 hours around (8 hours before and 16 hours after) the start time of the associated solar flare. In each case, the data were obtained from the NASA Coordinated Data Analysis Web (CDAW) website.[1]

The presence of an SEP event in each energy band was determined by first smoothing the flux data using a Savitsky–Golay filter to reduce the effect of small-scale variations. The flux was then examined to find the point at which it began to increase rapidly, with data prior to this point defined as the background. The onset times were then calculated using a Poisson cumulative sum (CUSUM) method (*cf.* Huttunen-Heikinmaa, Valtonen, and Laitinen, 2005). The CUSUM method is widely used in industry to identify changes in running processes, with a Poisson-CUSUM approach used if the data has a Poisson distribution. This approach works by cumulating the difference between an observed count Y_i and a reference value,

$$k = \frac{\mu_{\mathrm{d}} - \mu_{\mathrm{a}}}{\ln(\mu_{\mathrm{d}}) - \ln(\mu_{\mathrm{a}})}, \tag{1}$$

where μ_{a} is the mean of the background flux and μ_{d} is μ_a plus twice the standard deviation of the background flux. If this cumulation exceeds a threshold value h (chosen to minimise the effect of small point-to-point fluctuations while retaining sensitivity to large-scale particle events), then an out-of-control signal is given. In this case, a particle event was identified

---

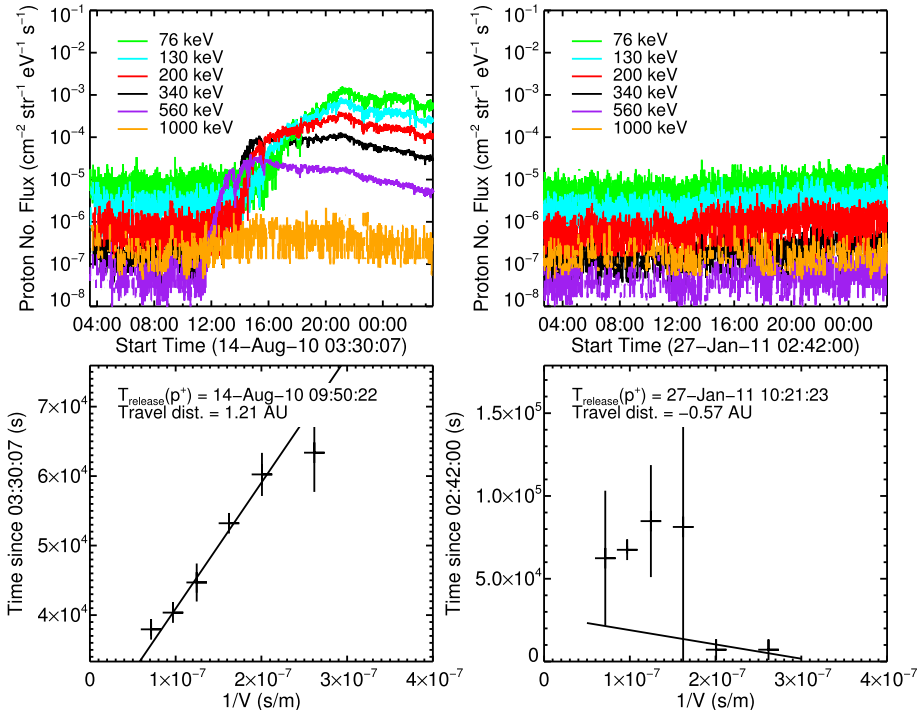[1]See http://cdaweb.sci.gsfc.nasa.gov/index.html/.

Figure 2 Proton flux (*top row*) and resulting velocity dispersion plots (*bottom row*) for a wave with an associated SEP event (14 August 2010; *left column*) and without an associated SEP event (27 January 2011; *right column*). SEP onset is detected automatically in each case (see main text), with the onset time in each energy band used to construct the velocity dispersion plot and estimate the time of particle acceleration on the Sun.

by looking for 300 out-of-control signals in a row. The onset time of particle detection at the spacecraft was then defined by the time of the first out-of-control signal.

Once an onset time was determined for each energy level, a velocity dispersion analysis was used to determine the release time of the particles from the Sun (*e.g.* Reames, 2009). This was also used to confirm the presence of an SEP event, with an event defined to have occurred if the velocity dispersion analysis gave a realistic physical release time from the Sun, *i.e.* the release time was before the onset time. An example of two events with realistic and unrealistic release times is shown in Figure 2. In the realistic case, the onset time at each energy can be identified by the sudden increase in particle flux, which corresponds to a valid estimate of release time and travel distance using the velocity dispersion plot. However, no such increase may be discerned in the unrealistic case, leading to the physically impossible estimates of release time and travel distance in the resulting velocity dispersion plot. Velocity dispersion analysis is a commonly used technique that assumes both that particles at all energies are released at the same time and that particle scattering is energy independent. However, energy dependent particle scattering can greatly affect particle arrival times, meaning that propagation through the heliosphere is not a simple trajectory along the Parker spiral. Therefore, to ensure consistency, each event was initially processed using this approach with the resulting plots examined "by eye" for confirmation.

2.3. Identification and Characterisation of Type II Radio Bursts

The type II radio bursts associated with each global wave event were identified using the daily lists of radio bursts collated by the Space Weather Prediction Centre located at the National Oceanic and Atmospheric Administration (NOAA/SWPC). A window 90 minutes either side of the start time of the global wave was used to look for associated events in the NOAA/SWPC list. This choice of time window was motivated by the fact that type II radio bursts can be seen up to 15 minutes before or after the first instance of an EUV wave observation (Park *et al.*, 2013; Warmuth, 2010; Miteva *et al.*, 2014); the larger time window used here was chosen to account for any anomalous events. For each candidate radio burst associated with a global wave, the SWPC list provides an associated start time, an end time, the observatory used to make the observation, the frequency range of the burst and the estimated drift speed. It should be noted that the drift speeds used in this analysis are the values provided by NOAA/SWPC, which are obtained using the standard approach of converting drift rate to speed *via* a density model of the solar corona (Mann and Classen, 1995; Miteva and Mann, 2007). However, it should be remembered that the absolute values of these bursts are known to be subject to large uncertainty given the often arbitrary nature of the models and the differences between individual observatories (Magdalenić *et al.*, 2008, 2012). This estimation also assumes a radially propagating shock driver, whereas it has been shown that shocks can often propagate non-radially (Mancuso and Raymond, 2004; Magdalenić *et al.*, 2012). Nonetheless, given the goal of trying to find a statistical correlation between radio burst properties and various other phenomena, we believe that the uncertainties associated with using the quoted type II burst speeds should be acknowledged but are not of major concern.

3. Results

Due to limitations inherent to the approach taken by CorPITA, it was not possible to analyse all of the events identified by Nitta *et al.* (2013) as they originated either too close to or beyond the solar limb. CorPITA requires a source point from which to track the pulse and so it cannot study events that do not originate on disk. As a result, of the 410 wave events identified by Nitta *et al.* (2013), only 362 could be analysed using CorPITA. 164 events were classified as having global waves by CorPITA, with no waves found for the remaining 198 events. The output from CorPITA for all events studied is listed in Table 1.

3.1. Wave Kinematics

The global waves identified here exhibited a wide variety in their kinematics, both from arc to arc within each event and from event to event. For a given event, CorPITA is designed to examine each arc sector separately, allowing the directional variation in pulse position to be identified and studied. Although this provides a more accurate estimate of how the wave evolves, it makes event-to-event comparison difficult as it raises the question of which velocity and acceleration values should be used. For every event studied here, the initial velocity and acceleration were calculated for each arc by first identifying the largest section of contiguous data-points exhibiting increasing distance away from the source point and fitting these points using a quadratic function (as illustrated in Figure 3 of Long *et al.*, 2014). The medians of the initial velocity and acceleration values across all arc sectors with a sufficiently high quality rating were then chosen as being most representative of the
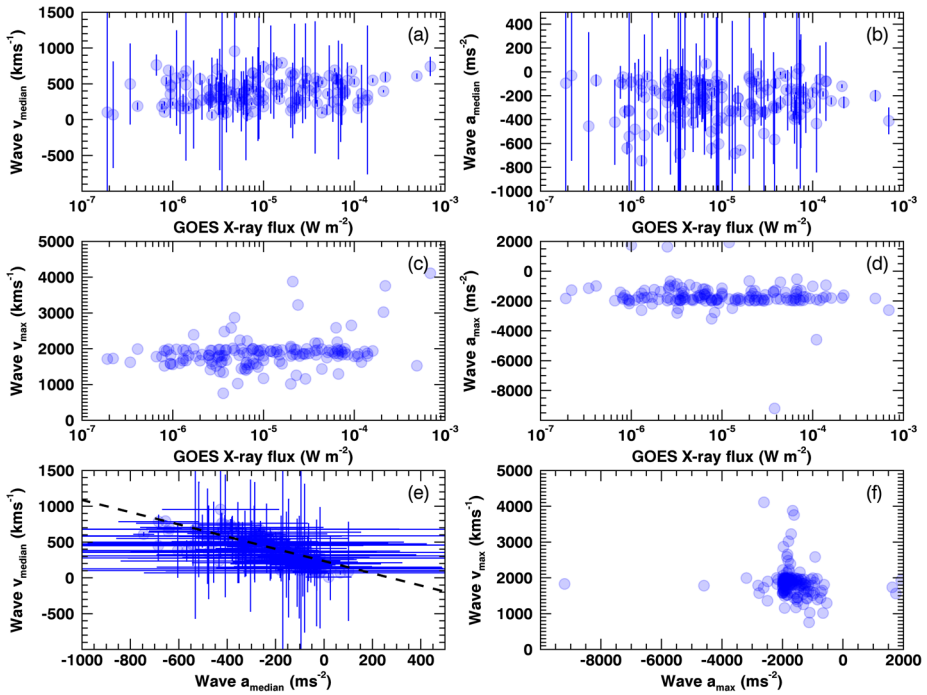
Figure 3 Relationship between the GOES X-ray flux of the associated flare and the median initial velocity (panel **a**), median acceleration (panel **b**), maximum initial velocity (panel **c**) and absolute maximum acceleration (panel **d**) of the wave measured by CorPITA. Bottom two panels show the relationship between the median velocity and acceleration of the wave (panel **e**) and maximum velocity and acceleration of the wave (panel **f**).

kinematics of that event. Panels a and b of Figure 3 show the median initial velocity and acceleration, respectively, of all events studied plotted with respect to the peak GOES X-ray flux of the associated flare in each case. It is clear that there is a broad spread in both the median initial velocity and the acceleration of the waves studied, with the maximum median initial velocity peaking at $\approx 950 \, \text{km}\,\text{s}^{-1}$ and the maximum median acceleration peaking at $\approx -750 \, \text{m}\,\text{s}^{-2}$.

To determine whether the median initial velocity and acceleration of the waves was most appropriate for comparing events, the maximum initial velocity and acceleration of the wave events were also examined. These were taken as the maximum of the initial velocity and acceleration values derived across all arc sectors with a sufficiently high quality rating for a given event. Panels c and d of Figure 3 show the maximum initial velocity and acceleration, respectively, of all events studied plotted with respect to the peak GOES X-ray flux of the associated flare in each case, similar to panels a and b of Figure 3. Although the maximum initial velocity and acceleration are clustered around $\approx 2000 \, \text{km}\,\text{s}^{-1}$ and $\approx -2000 \, \text{m}\,\text{s}^{-2}$, respectively, there is a much larger spread in both, as apparent from panels c and d of Figure 3.

Finally, the initial velocity and acceleration were plotted against each other for both the median and the maximum values to try and identify any trends comparable to those previously found by Warmuth (2010), Warmuth and Mann (2011) and Muhr *et al.* (2014). Panel e of Figure 3 shows the median initial velocity plotted against median acceleration for each event studied. It is possible to identify a clear trend in this case, with faster (slower) waves

exhibiting a stronger (weaker) negative acceleration. This is consistent with the results of both Warmuth and Mann (2011) and Muhr *et al.* (2014), who plotted the initial velocity against acceleration, and with Warmuth (2010), who plotted the average velocity against acceleration. The approach was repeated for the maximum initial velocity and acceleration (shown in Figure 3f), but consistent with panels c and d, the plot shows a much broader spread. Although a slightly decreasing trend can be discerned, with faster (slower) waves again exhibiting a stronger (weaker) negative acceleration, this trend is much weaker than that apparent for the median initial velocity and acceleration data shown in panel e. This suggests that the maximum initial velocity and acceleration are poor indicators of the overall wave kinematics and the median initial velocity and acceleration should be used when trying to characterise a given wave event using a single kinematic value.

Previous work by Warmuth and Mann (2011) used the wave catalogue of Thompson and Myers (2009) to suggest that there were three kinematic classes of global EUV waves. Class 1 referred to initially fast waves with a strong deceleration, class 2 waves had moderate and nearly constant speeds while class 3 referred to slow waves with an erratic kinematic profile. The results shown in Figure 3e are generally consistent with the results of Warmuth and Mann (2011), but it is not possible to distinguish three independent kinematic classes of global waves in this case. This may be due to the larger number of events used (164 here compared to 61 for Warmuth and Mann, 2011) or alternatively the higher cadence of SDO/AIA compared to SOHO/EIT and STEREO/EUVI in Warmuth and Mann (2011). However, when the data in Figure 3e were fitted using a linear relation, an intercept of $180 \ \mathrm{km \, s^{-1}}$ was found, consistent with the cutoff value of $\approx 170 \ \mathrm{km \, s^{-1}}$ used by Warmuth and Mann (2011) to define the difference between linear waves and those features possibly due to magnetic reconfiguration. However, this value was slightly lower than the intercept found by Muhr *et al.* (2014) using STEREO/EUVI observations. The consistency between the results presented here and by Warmuth (2010), Warmuth and Mann (2011) and Muhr *et al.* (2014) indicates that these features are large-amplitude events as outlined by Long *et al.* (2017).

Although the catalogue of Nitta *et al.* (2013) was used as a starting point for this work, it is worth noting that the analysis of the pulse kinematics described here and shown in Figure 3 do not match the results presented in Nitta *et al.* (2013). This is most likely due to the different approaches used to identify the wave pulse and measure its kinematics. Whereas Nitta *et al.* (2013) tracked the leading edge of the wavefront in a 2-dimensional time–distance plot, here a 1-dimensional intensity profile of the wavefront was fitted using a Gaussian, with the centroid of the Gaussian taken as the position of the wavefront at each point in time. This approach removes the effect of pulse broadening on the identified pulse position (see, *e.g.* Long *et al.*, 2014, for a more detailed discussion). In addition, both the velocity and the acceleration of the pulse were simultaneously measured here for each pulse using a single quadratic fit to the temporal variation in pulse position. This is in contrast to Nitta *et al.* (2013), who used both linear and quadratic fits independently applied to the temporal variation in pulse position to estimate the velocity and deceleration of the pulse, respectively.

3.2. Relationship with Solar Flares and Active Regions

When global EIT waves were first observed there was a lot of discussion regarding their origin, with the debate focusing on whether they were initially driven by the associated flare or coronal mass ejection (*e.g.* Cliver *et al.*, 2005; Vršnak *et al.*, 2006). Since then, the general consensus has been reached that they are initially driven by the rapid lateral expansion of the
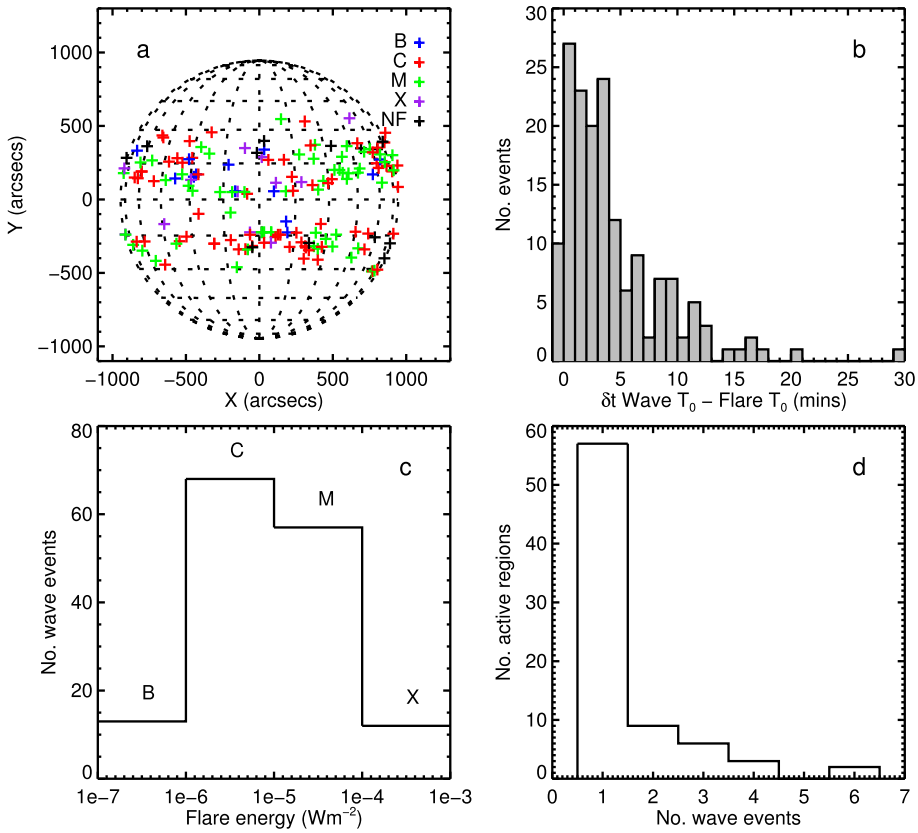
Figure 4 Panel **a** The location of every flare with an associated wave identified by CorPITA with colour indicating flare class. Panel **b** The relationship between the start time of the flare as defined by GOES and the time of the first wavefront observed by CorPITA. Panel **c** The number of global waves associated with each flare class. Panel **d** The relationship between active regions and global waves.

erupting CME in the low corona; a conclusion strongly supported by the SDO observations reported by Patsourakos, Vourlidas, and Stenborg (2010). A detailed discussion of the predictions made by the different theories and how recent observations support this conclusion may be found in the recent paper by Long *et al.* (2017).

As shown in panel a of Figure 4, all of the events studied here originated in the activity belts, consistent with previous observations (*e.g.* Muhr *et al.*, 2014). However, 14 of the events studied had no associated flare. The vast majority of the waves also tended to start after the start time of the associated flare, as indicated by panel b of Figure 4, although 10 events studied did start before the flare. While most of the waves identified were first observed by CorPITA within 10 minutes of the start of the flare, some were not observed until up to 30 minutes after the flare (as defined by the NOAA GOES catalogue). Panel c of Figure 4 indicates a broad spread in the size of the flares associated with each wave studied. Although the vast majority of waves were associated with M- and C-class flares, more than 10 waves were associated with both B- and X-class flares respectively.

These results suggest that the flare plays little-to-no role in the initiation or even existence of a wave, indicating that some other criteria must be fulfilled before a solar eruption pro-
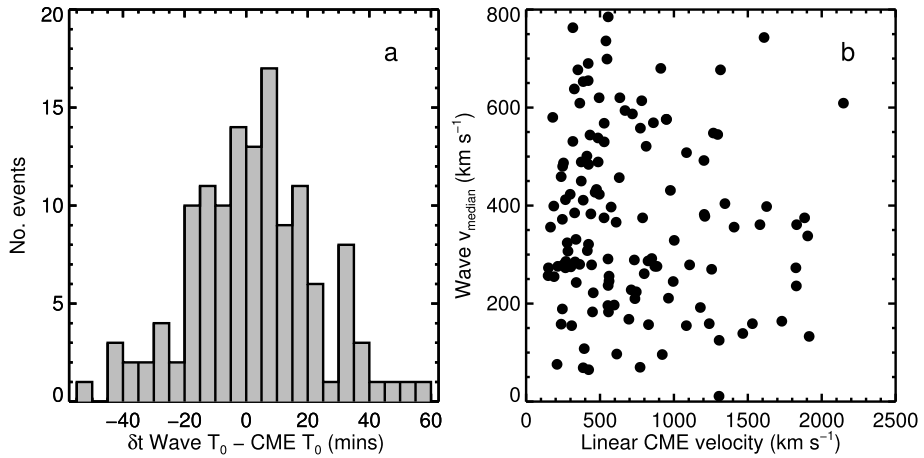
Figure 5 Panel **a** The relationship between the start time of the CME as defined by the linear fit to the temporal variation in CME position obtained from the LASCO CDAW catalogue and the start time of the wave detected by CorPITA. Panel **b** The relationship between the median initial wave velocity measured by CorPITA and the linear starting velocity of the CME measured by CDAW.

duces a wave. While the relationship with CMEs is examined more closely in Section 3.3, panel d of Figure 4 suggests that the active region from which the wave originates may be important. Over 25% of active regions produced more than one wave during their time on disk, with two active regions producing six waves each. This suggests that the magnetic structure of the active region or its relationship with the surrounding quiet solar corona may determine the ability of the active region to produce a wave during a solar eruption.

3.3. Relationship with CMEs

A comparison was also made between the identified waves and their associated coronal mass ejections as identified by the LASCO CDAW catalogue.[2] Global waves have historically been strongly associated with CMEs, with Biesecker *et al.* (2002) in particular suggesting that every wave has an associated CME while not every CME has an associated wave. However, a direct comparison between the on-disk global wave and the erupting CME is complicated by the fact that CMEs are best seen when in the plane of the sky (so when associated with eruptions close to the limb) whereas global waves are best observed and tracked on disk.

As shown in Figure 5, there is no clear correlation between the start time of the global wave and the start time of the associated CME predicted by the linear fit to the temporal variation in CME position obtained from the LASCO CDAW catalogue (panel a). Similarly, there is no clear correlation between the median initial wave velocity and the fitted linear velocity of the CME (panel b). While initially concerning, both of these results are consistent with our current understanding of global waves and CMEs and their relationship; a point worth discussing in more detail.

The CDAW catalogue uses LASCO observations to identify and measure CMEs and, as a consequence of the location of SOHO/LASCO at the L1 Lagrange point, is biased towards

---

[2]See https://cdaw.gsfc.nasa.gov/CME_list/.
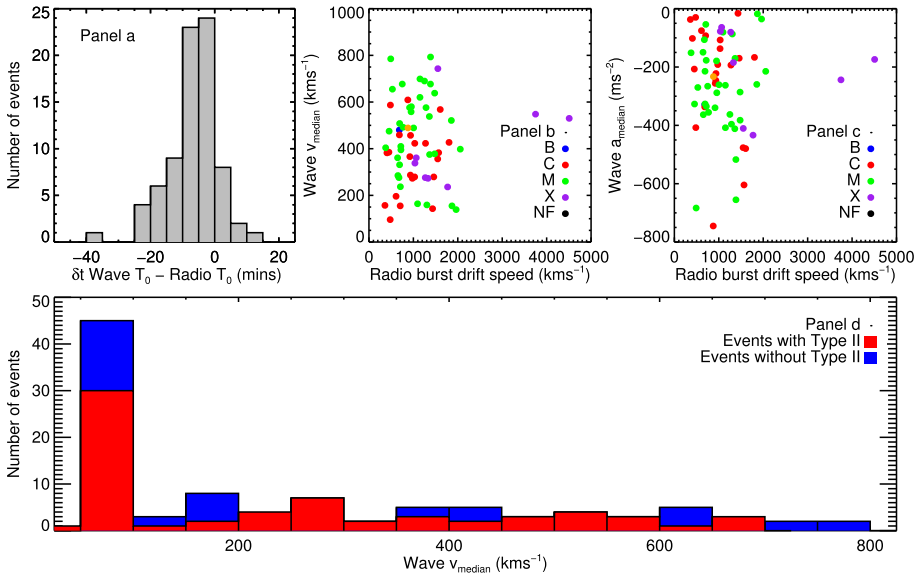
Figure 6 Panel **a** The offset time between the start of the global wave and the associated type II radio burst. The relationship between the median velocity (panel **b**) and median acceleration (panel **c**) of the wave as measured by CorPITA and the drift speed of the type II radio burst. Panel **d** Histogram showing the variation in median wave velocity for wave events with and without type II radio bursts.

CMEs erupting from the solar limb as seen from Earth. As a result, CMEs associated with global waves observed by SDO/AIA tend to be observed as halo CMEs, which are difficult to identify and measure. The velocity and starting time values used here were also taken from the linear fits to the temporal variation of the CME distance, with the result that any acceleration or deceleration of the CME was ignored, which may account for the spread in projected CME start times. Finally, the predicted mechanism by which the waves are produced by the lateral expansion of the erupting CME in the low corona suggests that there should be no direct correlation between the velocity of the wave and the forward velocity of the CME (which is what is typically measured when studying CMEs). As a result the lack of any correlation shown in Figure 5 is to be expected.

3.4. Relationship with Type II Radio Bursts

With the growing consensus on the interpretation of global coronal waves as large-amplitude waves initially driven by the lateral expansion of a CME in the low corona, a natural comparison can be made between global waves and type II radio bursts. Type II bursts are strongly associated with MHD shock waves (*cf.* Nelson and Melrose, 1985) and as a result the relationship between them and global waves has long been hypothesised and investigated (*e.g.* Cliver, Webb, and Howard, 1999; Biesecker *et al.*, 2002; Nitta *et al.*, 2014). However, their relationship remains inconclusive.

Despite the strong relationship between type II radio bursts and MHD shock waves and the interpretation of global EUV waves as large-amplitude or shock waves, a comparable number of wave events were identified with and without associated radio bursts. 66 wave events had an associated type II burst, with 98 wave events having no associated type II

radio signature detected at Earth, meaning that 40% of the waves in our sample have an associated type II burst. This is higher than the 22% association rate reported by Muhr *et al.* (2014), but comparable to the 43% association rate reported by Biesecker *et al.* (2002) for waves with a high quality rating ($> 50\%$ using the classification of Thompson and Myers, 2009). However, this is much lower than the 100% associated rate between type II bursts and EUV waves with an associated Hα Moreton–Ramsey wave reported by Warmuth *et al.* (2004) and Warmuth (2010). It should be noted that no comparison was made in this paper between global waves observed in EUV and Hα passbands; given the relative lack of recent synoptic studies of Moreton–Ramsey waves in Hα data we leave a more detailed analysis of the relationship between these two phenomena for a dedicated future work.

As shown in Figure 6d, there is no relationship between the median velocity of the wave and whether or not it had an associated type II burst, with very fast wave events exhibiting no type II emission while a significant number of very slow events had associated radio emission. This is most likely related to the fact that type II radio burst generation is related to conditions in the upper corona at $> 1.2\ R_\odot$ (Mann *et al.*, 2003), while the global wave propagates lower down in the corona (at $\approx 70 – 100$ Mm, *cf.* Kienreich, Temmer, and Veronig, 2009; Patsourakos and Vourlidas, 2009).

For those events which had an associated type II radio burst, the start of the radio emission was observed after the start of the wave in the vast majority of cases (see Figure 6a), similar to the relative start times of waves and radio bursts reported by Miteva *et al.* (2014) and Warmuth (2010). This delay between the start time of the global wave and the associated type II burst is likely due to the time taken for the disturbance to either become super-Alfvénic (as modelled by Vršnak and Lulić, 2000), or the time taken for the driver to reach regions of low ambient Alfvén speed in the corona (Mann *et al.*, 2003; Zucca *et al.*, 2014); in some cases this can take up to 30 minutes after detection of the wave. The duration of the radio bursts was also observed to be at most 35 minutes, with most radio bursts lasting less than 20 minutes, consistent with the lifetime of the observed waves. However, a number of events had associated radio emission which was observed to start prior to the first detection of the global wave, suggesting that the radio emission in those cases may have been due to either the rapid expansion of the CME rather than the wave, or the CME driving a shock radially before any lateral expansion produced the wave. In either case, the difference in start time of up to 30 minutes between the waves and associated type II radio bursts means that while they may originate from a common MHD disturbance in the corona, they most likely belong to spatially separated parts of this disturbance.

There is also no clear relationship between either the median initial velocity or acceleration of the identified waves and the drift speed of the associated radio bursts. Panels b and c of Figure 6 show that most of the events identified tended to have drift velocities of $0 – 2000$ km s^{-1}, with two notable exceptions in both cases. Some of the events also had quite high drift velocities of ≈ 2000 km s^{-1} despite estimated median velocities lower than 200 km s^{-1}. Even when accounting for the size of the associated flare, there is still no clear relationship between median initial wave velocity and drift speed of the associated type II burst, with the flare size in panels b and c of Figure 6 indicated by the colour of the data-point.

This lack of a clear relationship between the drift velocity of the type II burst and the median initial velocity of the identified wave is at odds with the conclusions of Warmuth (2010), who found a linear relationship between these parameters. Several individual case studies have also reported a kinematical relationship between type IIs (*e.g.* Vršnak *et al.*, 2006; Pohjolainen, Hori, and Sakurai, 2008; Grechnev *et al.*, 2011; Kozarev *et al.*, 2011; Ma *et al.*, 2011). However, there may be several reasons for the lack of such a relationship that

we find here. Firstly, as mentioned above, while the type II radio burst and the global wave are most likely different manifestations of the same shock in the corona, they may belong to separate parts of this shock, *i.e.* the wave propagates laterally or parallel to the solar surface, while the type II burst may propagate (semi-)radially (Grechnev *et al.*, 2011). Second, there is no guarantee that these speeds will be the same. In fact, the discrepancy between the type II drift speed and the wave speed means that expansion of the MHD disturbance is most likely anisotropic, with no relationship between lateral and radial expansion speed. Thirdly, a major issue with relating these two speeds concerns the reliability of the type II speed itself. This speed is derived from one of the many density models used in radio physics, which are often chosen arbitrarily and may not represent the density environment of the event (Magdalenić *et al.*, 2008). This analysis also assumes radial radio source propagation, which may not be the case. Finally, Warmuth (2010) focused on global EUV waves with associated Hα Moreton–Ramsey waves. Given the supposed mechanism by which these phenomena are thought to be related (*i.e.* the coronal EUV wave has a sufficiently large downward impulse that allows its footprint to be observed as a Moreton–Ramsey wave; see, *e.g.* Warmuth, 2010, 2015, for more details), this indicates that the waves observed by Warmuth (2010) were large-amplitude shocks. Although a similar mechanism may have produced the global waves studied here, these waves may not have been sufficiently strong to produce a radio signature. This suggests that a more granular study, focusing on strong EUV waves with associated Hα Moreton–Ramsey waves might provide a higher correlation between global EUV waves and type II radio emission (comparable to Warmuth *et al.*, 2004; Warmuth, 2010).

3.5. Relationship with Solar Energetic Particle Events

Similar to the predicted relationship with type II radio bursts, as large-amplitude and sometimes weakly shocked waves, global waves would be expected to accelerate solar energetic particles as they propagate across the Sun. However, of the 164 events with identified global waves, only 21 were found to have any evidence of an associated proton event, whereas only 14 events were found to have any evidence of an associated electron event (of which 12 had an associated proton event). While there are several probable reasons for this discrepancy, it is most likely due to a lack of connectivity between the field lines along which the particles could be accelerated and the spacecraft detecting the particles. In a simplistic interpretation, only events erupting from solar west would be expected to have any connectivity with the detecting spacecraft due to the Parker spiral, a suggestion consistent with the fact that 19 of the 23 events found here were associated with flares that originated on the western hemisphere.

However, recent studies have shown that even events on the far side of the Sun can produce particle detections at Earth, with studies by Rouillard *et al.* (2012) and Lario *et al.* (2016) suggesting that the global waves travelled across the Sun and eventually encountered field lines connected to Earth/L1. It has also been shown that particles can be detected despite being produced far from the footpoint of a magnetic field line connected to the spacecraft as a result of either super-radial spreading of field lines throughout the corona (*e.g.* Klein *et al.*, 2008), or very high levels of lateral diffusion in a turbulent solar wind (*e.g.* Laitinen *et al.*, 2016). The large spatial extent of global waves and their ability to accelerate particles far from the erupting active region therefore suggests that more SEP events should have been identified. However, only four events were found here that were associated with active regions located in the eastern solar hemisphere.

This lack of identified events may be due to the configuration of the coronal magnetic field into which the wave is propagating. Although previous work by Park *et al.* (2013, 2015) compared wave propagation to a potential field source surface extrapolation of the solar corona to compare the time at which the wave encountered a connected field line with the inferred SEP release times, this approach is rarely taken. However, the results described here suggest that a full understanding of the ability of a global wave to accelerate SEPs must combine the propagation of the wave with a full understanding of the coronal and heliospheric magnetic field. Although this approach is beyond the scope of the statistical path taken here, we hope to return to it in a dedicated future work.

4. Discussion and Conclusions

In this manuscript, we have applied the Coronal Pulse Identification and Tracking Algorithm (CorPITA) to the list of global coronal waves assembled by Nitta *et al.* (2013) and compared the output with a variety of other solar phenomena. Of the 410 events identified as waves by Nitta *et al.* (2013), only 362 could be processed using this approach due to requirements on the location of the source point of the wave. Of these 362 events processed, 164 were classified as having associated global waves, with CorPITA finding no waves for the remaining 198 events. This indicates a significant disconnect between the systematic automated approach to identifying and characterising global coronal waves and the traditional "by-eye" approach. Although most of these issues can and should be overcome through advanced image and signal processing and feature tracking, some may be due to the different definitions used to identify the wave pulse. For example, CorPITA uses a series of 1-dimensional intensity profiles obtained from percentage base-difference images to identify and fit the wave using a Gaussian model, whereas Nitta *et al.* (2013) used 2-dimensional distance–time stack plots to identify the leading edge of the pulse.

With the waves identified and tracked, the next step was to examine the variation in wave kinematics. As CorPITA uses a series of 360 10° arc sectors to identify and track the waves, each wave can be represented by a range of velocity and acceleration values which may not be representative of the large-scale motion of the wave. The maximum velocity and acceleration in particular are poorly representative of the overall wave motion as they can be strongly affected by anomalous measurements. However, the median velocity and acceleration provide a much better representation of the large-scale kinematics and should always be used when wishing to describe a wave using a single kinematic value. The median velocity and acceleration of the measured waves were also found to be correlated (consistent with the previous work of Warmuth and Mann, 2011). Although the spread in values increased with both velocity and acceleration, faster waves tend to have a stronger deceleration. However, no clear relationship could be determined for the maximum velocity and acceleration, suggesting that they are not representative of the overall kinematics of the wave.

There was also no clear relationship between the global waves and the associated solar flares. Neither the maximum or median velocities or accelerations showed any relationship with the class of the associated flare, with C-class flares associated with the waves that exhibited both the highest and the lowest median velocity. Similarly, there was no clear correlation between the wave parameters described here and the properties of the associated CMEs as measured by the LASCO CDAW catalogue. However, this is most likely due to instrumental and measurement effects rather than the lack of any underlying physical relationship and is unsurprising given the statistical approach taken here. A more thorough

analysis would require measurements of CMEs taken away from the Sun–Earth line and would measure the lateral expansion velocity rather than the forward motion of the CME. It was possible to observe CMEs propagating along the Sun–Earth line using the STEREO spacecraft, with the instruments on both spacecraft deliberately designed to have overlapping fields-of-view in the low corona which could allow the lateral expansion of the CME to be measured. However, the low temporal cadence of the instruments makes it difficult to disentangle the wave from the expanding CME, while the gradual progression of STEREO behind the Sun during the period of this project complicates a direct comparison between the global wave and the associated CME. Finally, no correlation was found between the global waves and SEPs, with only 21 of the events exhibiting any SEP signature. This is most likely because only *Wind* data were used in this analysis, but the ability of global waves to accelerate particles far from their erupting active region suggests that the structure of the coronal magnetic field into which the wave propagates should be accounted for when trying to study the acceleration of SEPs by global waves in the solar corona.

The lack of any clear statistical correlation between the different solar phenomena studied here indicates that determining the criteria required to produce a global wave is not a simple task. Although the majority of waves identified here were associated with both flares and CMEs, the parameters measured show no correlation, suggesting that the free energy available within an active region to produce a flare and accelerate the CME does not determine the presence of a wave in the subsequent eruption. However, it was found that over 25% of active regions produced multiple wave events, with two active regions producing six wave events each. This suggests that the structure of the erupting active region and its connectivity with the surrounding quiet solar corona may be much more important for determining the presence of a global wave in a solar eruption. Understanding the criteria required to produce a global wave therefore requires a more detailed examination of an active region producing multiple wave events, which we hope to continue in a dedicated future work.

Appendix

Table 1 below outlines the complete list of global wave events identified by Nitta *et al.* (2013) and processed by the CorPITA code for this paper. t_flare refers to the start time of the flare as defined by the GOES classification. t_wave refers to the time of the first observation of the wave by CorPITA. Num. arcs refers to the number of arcs in the largest segment in which CorPITA has identified a wave, with Central arc referring to the central arc of this segment in degrees clockwise from solar north. Median velocity is given in $\mathrm{km\,s^{-1}}$ and median acceleration is given in $\mathrm{m\,s^{-2}}$. The complete list is also available as a comma separated value list attached to the online version of this paper.

Table 1 CorPITA analysis.

Date	Flare X arcsec	Flare Y arcsec	t_{flare} UT	t_{wave} UT	Flare class	Active Region	Num. arcs	Central arc	Wave	Median initial vel.	Median acc.
12/06/2010	594.71	363.03	00:53:00	00:54:36	M2.0	11081	13	7	Yes	538±48	−412±39
12/06/2010	691.79	348.25	09:13:00	09:13:48	C6.1	11081	9	357	No	317±185	−361±90
13/06/2010	851.45	−400.41	05:33:00	05:34:12	M1.0	11079	10	339	No	433±0	−367±20
16/07/2010	302.43	−403.04	15:00:00	15:10:48	N/A	N/A	28	71	Yes	324±593	−155±535
27/07/2010	672.98	−332.74	08:45:00	08:44:48	N/A	N/A	13	48	Yes	366±191	−326±471
01/08/2010	−523.76	249.95	07:37:00	07:53:48	C3.2	11092	18	9	Yes	292±220	−110±90
07/08/2010	−454.63	58.73	17:59:00	18:00:48	M1.0	11093	17	182	Yes	276±19	−106±10
14/08/2010	772.31	170.44	09:30:00	09:30:36	C4.4	11099	18	183	Yes	382±33	−102±42
16/10/2010	397.8	−410.39	19:09:00	19:13:12	M2.9	11112	11	64	Yes	677±659	−517±1096
11/11/2010	−446.65	154.37	18:52:00	18:52:24	B9.4	11124	36	207	Yes	356±327	−322±311
11/11/2010	−430.27	170.73	19:40:00	19:55:48	C1.1	11123	29	263	Yes	581±658	−482±553
11/11/2010	−415.49	170.4	20:47:00	20:52:00	B9.0	11124	21	208	Yes	690±0	−639±49
13/11/2010	−209.41	236.37	17:04:00	17:17:48	B5.7	11125	9	205	No	493±255	−545±134
15/11/2010	626.35	−395.58	14:36:00	14:38:00	B7.6	11123	3	316	No	200±293	−159±1143
30/11/2010	−615.34	257.22	17:32:00	17:36:36	N/A	N/A	2	122	No	496±270	−689±155
15/12/2010	751.88	342.81	14:32:00	14:35:36	B2.2	11134	32	67	Yes	69±736	−31±711
31/12/2010	798.86	245.68	04:20:00	04:20:24	C1.3	11138	16	353	Yes	609±23	−745±41
27/01/2011	940.19	231.12	08:42:00	08:45:00	B6.6	11149	19	212	Yes	763±140	−422±352
13/02/2011	−63.96	−223.83	17:32:00	17:35:12	M6.6	11158	21	256	Yes	489±47	−261±58
14/02/2011	−63.54	−240.06	02:37:00	02:43:00	C1.6	11158	7	325	No	546±52	−341±36
14/02/2011	16	−223.22	04:39:00	04:41:12	C8.3	11158	7	35	No	648±209	−495±280
14/02/2011	16	−223.14	06:52:00	06:56:12	C6.6	11158	11	320	Yes	275±290	−287±205
14/02/2011	31.99	−223	12:42:00	12:41:36	C9.4	11158	4	38	No	298±393	−392±491
14/02/2011	79.9	−223.19	17:22:00	17:26:15	M2.2	11158	21	298	Yes	638±694	−286±437

Table 1 (*Continued.*)

Date	Flare X arcsec	Flare Y arcsec	t_{flare} UT	t_{wave} UT	Flare class	Active Region	Num. arcs	Central arc	Wave	Median initial vel.	Median acc.
14/02/2011	79.9	−223.12	19:25:00	19:31:12	C6.6	11158	11	338	Yes	474±141	−310±83
15/02/2011	110.22	−256.34	00:31:00	00:34:36	C2.7	N/A	12	319	Yes	550±309	−379±478
15/02/2011	190.57	−224.86	01:46:00	01:45:36	X2.2	11158	19	292	Yes	594±55	−256±45
15/02/2011	126.74	−240.04	03:10:00	03:12:24	N/A	N/A	4	50	No	301±405	−362±657
15/02/2011	142.45	−240.28	04:28:00	04:33:36	C4.8	N/A	13	279	Yes	955±678	−427±239
15/02/2011	−660.24	435.29	05:12:00	05:21:12	N/A	N/A	15	186	Yes	262±0	−136±22
15/02/2011	−653.92	421.52	07:11:00	07:13:36	N/A	N/A	5	214	No	207±0	−145±17
15/02/2011	252.6	−226.29	14:32:00	14:32:36	C4.8	11158	10	5	No	857±381	−615±494
16/02/2011	451.81	−268.73	14:21:00	14:22:00	M1.6	11158	16	16	Yes	793±4	−655±6
17/02/2011	654.81	−219.69	21:30:00	21:30:36	C1.1	11158	10	342	No	523±863	−485±1204
07/03/2011	−340.16	311.97	13:59:00	14:06:12	M1.9	11166	4	328	No	234±55	−82±21
07/03/2011	613.55	552.67	19:43:00	19:43:00	M3.7	11164	9	63	No	201±140	−113±734
08/03/2011	−859.25	−308.82	03:37:00	03:47:12	M1.5	11171	16	42	Yes	289±39	−220±63
08/03/2011	16.68	287.69	18:56:00	18:58:14	M4.4	11165	7	104	No	710±295	−398±190
12/03/2011	567.29	181.88	04:33:00	04:33:48	M1.3	11166	11	163	Yes	475±456	−327±749
12/03/2011	607.21	177.9	15:20:00	15:21:36	C9.6	11166	7	16	No	583±190	−695±458
24/03/2011	−647.65	−167.32	12:01:00	12:12:00	M1.0	11176	14	51	Yes	736±78	−386±126
25/03/2011	−414.04	−98.05	23:12:00	23:12:00	M1.0	11176	8	13	No	533±51	−359±142
27/03/2011	−196.38	−89.83	00:07:00	00:11:02	C3.1	11176	19	67	Yes	705±138	−381±377
11/05/2011	713.56	324.45	02:18:00	02:18:12	B8.1	11204	14	17	Yes	224±21	−103±34
15/05/2011	683.11	210.36	23:28:00	23:31:02	C4.8	11208	19	251	Yes	499±86	−344±54
29/05/2011	−796.53	−348.34	10:10:00	10:11:12	M1.4	11226	10	30	No	274±50	−141±84
29/05/2011	−835.66	−287.02	21:00:00	21:03:36	C8.7	11227	30	327	Yes	356±647	−476±931
30/05/2011	−780.88	−285.79	10:48:00	10:50:00	C2.8	11227	7	4	No	219±52	−127±26

Table 1 (*Continued.*)

Date	Flare X arcsec	Flare Y arcsec	t_{flare} UT	t_{wave} UT	Flare class	Active Region	Num. arcs	Central arc	Wave	Median initial vel.	Median acc.
01/06/2011	−543.21	−284.33	02:44:00	02:56:48	C2.6	11228	31	61	Yes	327 ± 170	−111 ± 97
01/06/2011	−564.62	−301.12	16:30:00	16:32:00	C2.9	11226	9	231	No	163 ± 453	−75 ± 173
02/06/2011	−307.05	−300.72	06:25:00	06:27:00	C1.4	11227	25	305	Yes	487 ± 13	−213 ± 17
02/06/2011	−307.05	−300.72	07:35:00	07:41:02	C3.7	11227	36	289	Yes	431 ± 160	−198 ± 143
07/06/2011	715.5	−339.79	06:21:00	06:20:48	M2.5	11226	61	316	Yes	270 ± 49	−16 ± 17
11/07/2011	−94.7	−338.06	10:28:00	10:29:48	C2.6	11249	23	346	Yes	273 ± 40	−192 ± 49
30/07/2011	−525.23	170.96	02:06:00	02:18:48	M9.3	11261	6	196	No	182 ± 859	−51 ± 310
02/08/2011	221.76	153.91	05:50:00	05:58:36	M1.4	11261	9	149	No	483 ± 95	−156 ± 86
04/08/2011	545.89	200.45	03:44:00	03:44:00	M9.3	11261	20	214	Yes	677 ± 28	−266 ± 33
08/08/2011	811.74	214.5	18:00:00	18:01:12	M3.5	11263	10	93	No	690 ± 150	−523 ± 290
09/08/2011	865.98	228.62	08:00:00	08:03:36	X6.9	11263	13	206	Yes	743 ± 127	−410 ± 108
10/08/2011	−730.13	265.57	15:50:00	15:50:24	C1.5	N/A	10	185	No	398 ± 717	−257 ± 419
06/09/2011	112.99	113.33	01:40:00	01:41:24	M5.3	11283	16	57	Yes	614 ± 416	−237 ± 248
06/09/2011	286.52	118.11	22:15:00	22:15:36	X2.1	11283	16	67	Yes	397 ± 10	−120 ± 11
07/09/2011	435.27	126.02	22:32:00	22:36:48	X1.8	11283	6	48	No	228 ± 89	−50 ± 97
08/09/2011	595.76	139.64	15:35:00	15:41:36	M6.7	11283	13	185	Yes	276 ± 821	−146 ± 662
09/09/2011	671.39	182.12	06:03:00	06:03:24	M2.7	11283	19	183	Yes	410 ± 452	−177 ± 269
22/09/2011	−923.68	179.3	10:29:00	10:46:24	X1.4	11302	18	150	Yes	338 ± 16	−78 ± 8
23/09/2011	666.72	382.76	12:10:00	12:10:48	C3.2	11296	11	68	Yes	321 ± 0	−231 ± 60
23/09/2011	−848.96	149.29	23:48:00	23:59:12	M1.9	11302	8	149	No	388 ± 100	−217 ± 91
24/09/2011	−827.34	144.08	09:32:00	09:36:24	X1.9	11302	10	172	No	272 ± 107	−107 ± 84
24/09/2011	−801.49	189.78	12:25:00	12:25:24	M7.1	11302	19	306	Yes	133 ± 436	27 ± 464
24/09/2011	−801.55	189.87	19:09:00	19:17:26	M3.0	11302	8	357	No	486 ± 146	−262 ± 209
24/09/2011	766.09	−489.54	21:23:00	21:24:48	M1.2	11303	6	28	No	195 ± 82	−130 ± 200
24/09/2011	772.18	−487.88	23:50:00	23:53:24	M1.0	11303	17	353	Yes	183 ± 18	−129 ± 18

Table 1 (*Continued.*)

Date	Flare X arcsec	Flare Y arcsec	t_{flare} UT	t_{wave} UT	Flare class	Active Region	Num. arcs	Central arc	Wave	Median initial vel.	Median acc.
25/09/2011	783.63	−484.51	02:27:00	02:29:12	M4.4	11302	19	34	Yes	97±8	−12±9
25/09/2011	−718.52	124.7	04:31:00	04:47:12	M7.4	11302	41	165	Yes	375±172	−161±473
25/09/2011	803.65	−477.66	09:35:00	09:42:48	M1.5	11303	8	329	No	155±51	−72±68
25/09/2011	−637.55	131.42	15:26:00	15:26:00	M3.7	11302	6	157	No	591±287	−390±320
26/09/2011	−465.87	133.36	14:37:00	14:38:00	M2.6	11302	10	197	No	221±1424	−232±837
27/09/2011	−148.07	53.79	20:44:00	20:46:12	C6.4	11302	12	213	Yes	150±710	−102±587
29/09/2011	180.69	55.62	12:07:00	12:07:48	C2.7	11302	3	207	No	64±786	−36±2156
30/09/2011	494.2	137.52	02:46:00	02:57:24	C1.0	11302	16	181	Yes	224±20	−85±70
30/09/2011	−164.47	55.73	03:50:00	03:50:48	C7.7	11305	19	104	Yes	111±0	−180±10
30/09/2011	−82.81	38.18	18:55:00	19:06:15	M1.0	11305	19	227	Yes	331±109	−215±133
01/10/2011	99.05	55.61	09:40:00	09:40:24	M1.2	11305	10	242	No	440±79	−153±208
02/10/2011	229.25	58.79	00:40:00	00:41:36	M3.9	11305	6	141	No	439±27	−210±17
02/10/2011	400.46	66.5	21:40:00	21:44:12	C7.6	11305	25	218	Yes	653±222	−502±219
03/10/2011	835.05	114.3	02:08:00	02:08:48	C2.1	11302	6	78	No	175±60	−241±32
10/10/2011	−49.19	−317.22	14:30:00	14:37:12	C4.5	11313	6	128	No	710±210	−419±233
21/10/2011	944.23	84.68	12:55:00	12:57:12	M1.3	11319	8	237	No	218±704	−156±328
22/10/2011	851.81	387.66	10:10:00	10:13:24	M1.3	11314	6	291	No	201±116	−121±128
09/11/2011	−456.66	283.17	13:04:00	13:19:12	M1.1	11342	10	19	No	453±145	−229±185
14/11/2011	802.37	342.12	09:18:00	09:21:12	C5.2	11348	18	340	Yes	196±90	−75±308
15/11/2011	−481.92	92.97	00:08:00	00:10:48	N/A	N/A	8	137	No	300±352	−177±249
25/11/2011	317.28	−327.12	00:26:00	00:35:24	N/A	N/A	6	173	No	301±121	−95±63
25/11/2011	822.07	272.46	21:49:00	21:52:00	C2.4	11359	7	123	No	508±1198	−356±611
13/12/2011	−194.54	−276.36	03:08:00	03:10:24	N/A	N/A	7	42	No	602±466	−509±453
22/12/2011	286.05	−291.87	01:56:00	01:56:36	C5.4	11381	11	328	Yes	366±65	−256±207
25/12/2011	312.63	−318.46	08:49:00	08:49:12	C5.5	11387	32	26	Yes	286±25	−186±91

Table 1 (*Continued.*)

Date	Flare X arcsec	Flare Y arcsec	t_{flare} UT	t_{wave} UT	Flare class	Active Region	Num. arcs	Central arc	Wave	Median initial vel.	Median acc.
25/12/2011	397.89	−335.21	18:11:00	18:40:39	M4.0	11387	18	299	Yes	532 ± 72	−301 ± 39
25/12/2011	371.75	−318.46	20:23:00	20:26:48	C7.7	11387	27	275	Yes	648 ± 0	−643 ± 49
26/12/2011	497.64	−320.58	02:13:00	02:14:00	M1.5	11387	13	21	Yes	484 ± 57	−221 ± 100
26/12/2011	32.51	339.47	11:23:00	11:23:00	C5.7	11384	29	316	Yes	210 ± 33	−70 ± 53
27/12/2011	−496.06	−253.16	04:06:00	04:12:12	C8.9	11386	24	320	Yes	261 ± 0	−31 ± 12
23/01/2012	309.43	531.07	03:32:00	03:34:00	M8.7	11401	7	257	No	225 ± 76	−74 ± 150
27/01/2012	857.4	453.53	18:05:00	18:04:48	X1.7	11402	10	257	No	287 ± 20	−137 ± 20
04/03/2012	−832.64	332.2	10:29:00	10:29:36	M2.0	11429	13	185	Yes	125 ± 231	−38 ± 1256
05/03/2012	−764.07	362.1	03:34:00	03:37:12	X1.1	11429	24	217	Yes	159 ± 38	−136 ± 25
07/03/2012	−475.08	397.08	00:02:00	00:05:12	X5.4	11429	10	39	No	644 ± 347	−204 ± 152
07/03/2012	−396.04	356.26	01:00:00	01:02:48	X1.3	11430	34	109	Yes	273 ± 0	−185 ± 17
09/03/2012	32.37	398.16	03:35:00	03:35:36	M6.3	N/A	30	196	Yes	576 ± 78	−396 ± 201
10/03/2012	378.95	372.1	17:17:00	17:19:00	M8.4	N/A	11	180	Yes	545 ± 248	−298 ± 209
13/03/2012	803.97	352.08	17:12:00	17:14:00	M7.9	11429	14	339	Yes	375 ± 98	−170 ± 67
14/03/2012	−98.24	349.15	15:06:00	15:08:48	M2.8	11432	14	167	Yes	501 ± 55	−335 ± 38
17/03/2012	384.23	−226.55	20:32:00	20:34:00	M1.4	11434	9	22	No	690 ± 7	−403 ± 14
05/04/2012	487.41	364.33	20:49:00	20:52:48	C1.5	11450	36	343	Yes	157 ± 28	−37 ± 26
09/04/2012	821.5	306.67	12:12:00	12:13:24	C3.9	N/A	31	284	Yes	96 ± 265	−30 ± 622
19/04/2012	336.6	−346.26	11:06:00	11:08:48	C7.0	N/A	14	239	Yes	423 ± 14	−107 ± 6
23/04/2012	271.64	305.81	17:38:00	17:38:48	C2.0	11461	21	230	Yes	568 ± 78	−480 ± 50
24/04/2012	−919.02	211.19	07:38:00	07:37:48	C3.7	N/A	13	76	Yes	279 ± 63	−137 ± 327
30/04/2012	889.69	−298.98	06:56:00	06:56:24	C3.9	N/A	3	102	No	197 ± 92	−174 ± 53
17/05/2012	904.1	190.4	01:25:00	01:29:12	M5.1	11476	12	6	Yes	361 ± 26	−149 ± 13
01/06/2012	914.17	198.04	22:20:00	22:23:36	C3.3	N/A	23	302	Yes	457 ± 45	−222 ± 78
03/06/2012	−558.51	281.12	17:50:00	17:51:12	M3.3	N/A	8	339	No	135 ± 1156	41 ± 1275

Table 1 (*Continued.*)

Date	Flare X arcsec	Flare Y arcsec	t_{flare} UT	t_{wave} UT	Flare class	Active Region	Num. arcs	Central arc	Wave	Median initial vel.	Median acc.
06/06/2012	78.67	−294.38	19:54:00	19:53:36	M2.1	11494	15	160	Yes	620±168	−263±88
08/06/2012	337.97	−296.43	03:00:00	03:01:36	C7.7	N/A	20	150	Yes	531±144	−281±83
02/07/2012	−140.93	−339.38	05:03:00	05:03:47	C3.5	11515	15	168	Yes	279±1316	−170±1291
02/07/2012	−78.52	−340.2	10:43:00	10:44:11	M5.6	11514	8	22	No	366±351	−226±190
02/07/2012	−47.41	−325.5	19:59:00	20:01:47	M3.8	11515	17	155	Yes	375±143	−567±569
04/07/2012	511.39	200.98	16:33:00	16:38:38	M1.8	11513	8	221	No	306±795	−153±773
04/07/2012	425.08	−322.74	22:03:00	22:02:47	M4.6	N/A	8	45	No	527±108	−160±136
06/07/2012	786.25	−257.45	23:01:00	23:01:35	X1.1	N/A	16	130	Yes	236±108	−434±404
08/07/2012	912.05	−232.97	16:23:00	16:23:47	M6.9	11514	5	159	No	135±11	−176±33
12/07/2012	32.08	−294.69	16:09:00	16:08:59	X1.4	11522	11	356	Yes	276±1031	−81±325
23/07/2012	205.97	−323.53	01:35:00	01:35:47	N/A	N/A	2	3	No	142±687	−25±1612
28/07/2012	−704.99	−417.83	20:47:00	20:47:47	M6.1	11532	17	186	Yes	690±19	−363±30
31/07/2012	−809.27	251.46	10:50:00	10:50:11	M5.7	N/A	6	201	No	175±181	−104±152
06/08/2012	−912.72	−237.79	04:35:00	04:36:47	M1.6	N/A	5	93	No	449±622	−517±690
06/08/2012	−910.99	−239.53	08:15:00	08:16:59	C6.3	11532	5	33	No	183±597	−147±427
13/08/2012	61.05	269.02	12:33:00	12:35:59	C2.8	N/A	10	95	No	563±0	−505±8
14/08/2012	167	270.23	00:23:00	00:26:59	C3.5	11543	26	13	Yes	620±83	−437±125
15/08/2012	369.83	276.97	03:37:00	03:40:47	B8.5	11543	12	351	Yes	544±41	−334±49
16/08/2012	562.31	290.31	12:47:00	12:48:23	C3.6	11543	15	13	Yes	155±101	−93±136
17/08/2012	771.64	319.88	22:30:00	22:32:11	B5.9	N/A	6	51	No	42±537	−10±636
31/08/2012	−641.4	−444.23	19:35:00	19:43:23	C8.4	11560	9	40	No	178±37	−106±46
15/09/2012	839.48	392.98	22:53:00	22:56:11	B9.5	N/A	20	344	Yes	480±88	−329±146
16/09/2012	854.08	254.21	22:07:00	22:07:11	N/A	N/A	8	348	No	329±233	−224±190
10/11/2012	−153.03	−461.26	04:40:00	04:41:11	N/A	N/A	10	39	No	456±79	−264±122
18/11/2012	361.46	97.38	04:00:00	04:05:59	C5.7	11615	14	205	Yes	255±412	−111±244

Table 1 (*Continued.*)

Date	Flare X arcsec	Flare Y arcsec	t_{flare} UT	t_{wave} UT	Flare class	Active Region	Num. arcs	Central arc	Wave	Median initial vel.	Median acc.
20/11/2012	−267.76	50.36	19:23:00	19:27:35	M1.6	11618	15	231	Yes	436 ± 120	−332 ± 68
21/11/2012	−185.39	50.6	06:45:00	06:45:35	M1.4	11618	13	209	Yes	395 ± 112	−335 ± 198
21/11/2012	−101.57	50.88	15:15:00	15:15:49	M3.5	N/A	10	178	No	599 ± 889	−432 ± 494
24/11/2012	468.3	111.24	13:33:00	13:33:47	C3.3	11618	11	337	Yes	459 ± 311	−337 ± 866
05/12/2012	−903.96	283.49	00:09:00	00:17:23	C1.7	N/A	18	141	Yes	211 ± 607	−111 ± 432
07/12/2012	906.41	300.97	09:02:00	09:02:47	B4.7	N/A	3	132	No	459 ± 800	−443 ± 803
04/01/2013	523.52	−239.44	08:30:00	08:33:23	C1.3	N/A	16	328	Yes	158 ± 34	−100 ± 41
05/01/2013	418.31	−166.49	16:23:00	16:26:35	C1.3	N/A	14	54	Yes	257 ± 94	−158 ± 51
06/01/2013	740.84	−232.35	06:20:00	06:28:23	N/A	N/A	11	63	Yes	221 ± 124	−119 ± 256
09/01/2013	147.21	546.49	14:37:00	14:38:47	N/A	N/A	4	106	No	372 ± 473	−238 ± 877
11/01/2013	−573.1	142.66	09:02:00	09:07:35	M1.2	N/A	5	120	No	606 ± 109	−459 ± 174
12/01/2013	182.11	−149.8	06:10:00	06:11:35	N/A	N/A	4	166	No	284 ± 1281	−277 ± 1398
13/01/2013	348.76	367.75	08:35:00	08:35:23	M1.7	N/A	7	104	No	326 ± 46	−175 ± 75
18/01/2013	−478.54	273.78	17:03:00	17:05:11	C2.3	N/A	10	96	No	333 ± 601	−248 ± 448
06/02/2013	−324.37	457.08	00:04:00	00:20:14	C8.8	11667	7	11	No	705 ± 209	−834 ± 206
19/02/2013	−16.63	317.02	00:35:00	00:35:23	N/A	N/A	7	209	No	136 ± 0	−49 ± 130
30/03/2013	−731.85	267.14	13:07:00	13:07:23	B4.7	N/A	6	322	No	93 ± 0	−71 ± 116
11/04/2013	−244.94	259.8	06:55:00	06:58:14	M6.5	11719	31	257	Yes	569 ± 54	−299 ± 60
18/04/2013	937.1	172.74	17:56:00	18:01:11	C6.5	N/A	22	254	Yes	423 ± 58	−194 ± 53
20/04/2013	485.61	−208.67	01:03:00	01:06:47	B8.1	N/A	17	76	Yes	108 ± 13	−43 ± 18
20/04/2013	−32.73	282.95	07:54:00	08:00:23	C1.4	N/A	11	265	Yes	680 ± 1245	−532 ± 841
21/04/2013	179.52	264.02	06:50:00	06:50:35	N/A	N/A	8	110	No	119 ± 538	−108 ± 2543
21/04/2013	745.27	−248.66	19:59:00	20:03:35	C2.7	11726	19	264	Yes	246 ± 71	−65 ± 131
23/04/2013	885.79	−313.35	18:10:00	18:11:35	C3.0	N/A	6	256	No	274 ± 190	−282 ± 299
28/04/2013	547.06	−239.02	20:13:00	20:14:11	C4.4	11731	4	114	No	409 ± 1050	−157 ± 555

Table 1 (*Continued.*)

Date	Flare X arcsec	Flare Y arcsec	t_{flare} UT	t_{wave} UT	Flare class	Active Region	Num. arcs	Central arc	Wave	Median initial vel.	Median acc.
29/04/2013	705.73	−251.52	19:26:00	19:27:59	C4.0	11733	3	290	No	511±0	−758±81
01/05/2013	−176.17	312.46	02:30:00	02:30:11	N/A	N/A	3	120	No	672±79	−659±83
02/05/2013	396.34	241.81	04:58:00	04:58:47	M1.1	11731	6	36	No	199±71	−146±453
03/05/2013	−910.28	254.42	17:24:00	17:27:11	M5.7	N/A	3	64	No	230±254	−77±208
10/05/2013	285.91	278.64	16:30:00	16:31:47	C2.5	11739	22	302	Yes	286±167	−198±385
13/05/2013	−926.8	185.71	15:48:00	15:51:47	X2.8	N/A	6	24	No	600±38	−344±66
14/05/2013	−908.44	191.16	01:01:00	01:07:59	X3.2	N/A	7	353	No	466±7	−152±5
15/05/2013	−852.25	198.74	01:25:00	01:26:59	X1.2	11748	10	315	No	205±0	−197±4
17/05/2013	−549.09	213.01	08:43:00	08:49:11	M3.2	11748	15	8	Yes	404±137	−151±89
22/05/2013	875.33	238.26	13:05:00	13:08:59	M5.0	11747	24	245	Yes	139±57	−36±16
05/06/2013	622.17	−486.73	08:27:00	08:30:11	M1.3	11762	10	82	No	391±298	−291±166
07/06/2013	791.85	−501.35	22:33:00	22:34:23	M5.9	N/A	8	293	No	597±144	−839±157
21/06/2013	−868.58	−268.4	02:45:00	02:46:11	M2.9	11777	5	60	No	130±82	−27±82
23/06/2013	−806.35	−259.99	20:51:00	20:56:11	M2.9	11778	22	179	Yes	243±197	−118±145
09/07/2013	−233.19	234.6	14:15:00	14:18:35	B7.6	N/A	18	335	Yes	183±32	−88±133
15/07/2013	−330.79	−277.69	03:10:00	03:19:23	C3.0	11791	17	283	Yes	412±169	−207±103
15/07/2013	−254.46	−280.14	10:28:00	10:27:47	C3.6	11791	25	236	Yes	76±35	−57±70
18/07/2013	−892.56	−215.28	17:56:00	17:57:23	C2.3	N/A	5	339	No	251±540	−351±652
26/07/2013	412.53	−194.47	21:35:00	21:37:47	C1.8	N/A	13	300	Yes	220±59	−156±28
08/08/2013	436.82	−451.61	17:56:00	18:04:35	B4.1	N/A	13	298	Yes	189±44	−72±47
30/08/2013	−606.71	141.8	02:04:00	02:15:23	C8.3	11836	10	56	No	272±784	−166±881
19/09/2013	−554.57	−259.83	02:45:00	02:54:47	N/A	N/A	30	27	Yes	280±34	−150±59
29/09/2013	419.57	166.1	21:37:00	21:39:35	C1.2	N/A	18	21	Yes	192±387	−68±170
11/10/2013	−156.42	249.05	07:03:00	07:08:23	M1.5	11865	3	221	No	98±155	−20±84
22/10/2013	0	−4.01	21:15:00	21:15:59	M4.2	11875	5	94	No	505±107	−858±401

Table 1 (*Continued.*)

Date	Flare X arcsec	Flare Y arcsec	t_{flare} UT	t_{wave} UT	Flare class	Active Region	Num. arcs	Central arc	Wave	Median initial vel.	Median acc.
24/10/2013	−132.73	−252.06	00:21:00	00:22:13	M9.3	11877	9	179	No	348±27	−179±44
25/10/2013	−934.96	−151.27	02:48:00	02:51:35	M2.9	N/A	5	38	No	390±380	−138±103
25/10/2013	−914.49	−158.35	07:55:00	08:08:47	X1.7	N/A	4	160	No	368±129	−197±91
25/10/2013	−898.88	−162.4	14:53:00	15:05:11	X2.1	N/A	10	6	No	664±206	−243±90
28/10/2013	917	42.44	01:50:00	01:52:59	X1.0	11875	8	58	No	235±201	−98±162
28/10/2013	905.1	108.25	04:32:00	04:34:23	M5.1	11877	7	110	No	290±206	−127±87
28/10/2013	−451.62	−187.47	15:07:00	15:09:50	M4.4	11882	15	349	Yes	521±19	−260±55
05/11/2013	−659.41	−247.36	22:07:00	22:17:11	X3.3	11890	4	165	No	896±966	−535±737
07/11/2013	−442.52	−288.72	03:36:00	03:38:23	M2.3	11890	5	180	No	735±781	−308±563
08/11/2013	−228.19	−292.51	04:20:00	04:24:23	X1.1	11890	5	358	No	360±178	−131±83
10/11/2013	228.3	−289.11	05:08:00	05:11:26	X1.1	11890	7	296	No	468±152	−171±112
19/11/2013	884.14	−232.21	10:16:00	10:19:35	X1.0	11983	8	203	No	340±120	−147±108
01/12/2013	461.59	306.99	19:35:00	19:42:47	N/A	N/A	16	15	Yes	256±13	−89±11
05/12/2013	368.84	−256.92	20:30:00	20:32:59	N/A	N/A	4	144	No	197±321	−21±175
07/12/2013	708.26	−269.93	07:17:00	07:18:23	M1.2	11909	12	303	Yes	508±157	−327±301
12/12/2013	646.9	−375.81	03:08:00	03:10:47	C4.6	11912	21	41	Yes	329±361	−222±224
06/01/2014	180.56	−194.54	07:41:00	07:42:35	N/A	N/A	3	344	No	63±50	−31±129
07/01/2014	198.46	−158.5	18:04:00	18:05:23	X1.2	N/A	17	125	Yes	361±397	−64±280
08/01/2014	953.95	191.28	03:41:00	03:46:23	M3.6	11947	5	211	No	526±9	−811±18
20/01/2014	−130.27	367.31	19:23:00	19:27:47	N/A	N/A	5	51	No	345±337	−310±1471
26/01/2014	−164.11	−161.62	08:26:00	08:26:35	C1.5	N/A	7	141	No	371±137	−538±74
11/02/2014	−279.13	−96.02	03:25:00	03:30:14	M1.7	11974	6	336	No	365±195	−251±172
11/02/2014	−133.35	−74.84	16:34:00	16:38:11	M1.8	11974	3	90	No	172±593	−82±712
12/02/2014	−33.32	−90.4	04:15:00	04:24:47	M3.7	11974	11	42	Yes	450±915	−304±464
12/02/2014	401.63	318.5	12:15:00	12:16:23	N/A	N/A	45	337	Yes	291±30	−130±45

Table 1 (*Continued.*)

Date	Flare X arcsec	Flare Y arcsec	t_{flare} UT	t_{wave} UT	Flare class	Active Region	Num. arcs	Central arc	Wave	Median initial vel.	Median acc.
14/02/2014	403.17	−99.25	02:40:00	02:40:23	M2.3	11974	13	348	Yes	433±0	−310±46
16/02/2014	−33.41	−70.14	09:20:00	09:19:23	M1.2	11977	8	135	No	385±161	−500±268
17/02/2014	82.46	−120.81	02:51:00	03:02:23	C6.6	11977	10	276	No	177±719	−136±1517
17/02/2014	167.64	249.11	04:50:00	04:50:47	N/A	N/A	5	53	No	135±0	−69±13
18/02/2014	−517.99	−272.77	00:40:00	00:43:35	N/A	N/A	7	345	No	43±1108	22±1792
20/02/2014	−581.55	−142.83	03:15:00	03:23:23	C3.3	11982	13	191	Yes	143±840	−16±426
20/02/2014	897.2	−215.97	07:35:00	07:35:23	M3.0	11982	22	345	Yes	576±65	−340±55
25/02/2014	−939.12	−183.59	00:39:00	00:38:59	X4.9	11990	24	163	Yes	609±30	−200±43
04/03/2014	276.64	330.83	18:20:00	18:23:47	C5.5	N/A	2	50	No	325±134	−154±76
05/03/2014	292.32	330.17	13:20:00	13:28:59	N/A	N/A	7	144	No	34±605	−7±195
10/03/2014	−180.29	333.18	14:25:00	14:30:11	N/A	N/A	4	346	No	66±0	−26±12
12/03/2014	−238.52	408.81	14:00:00	14:01:11	N/A	N/A	2	32	No	135±0	−20±33
16/03/2014	−666.38	−284.79	02:52:00	02:53:23	N/A	N/A	15	154	Yes	197±44	−29±44
17/03/2014	−804.84	−310.35	12:08:00	12:12:59	N/A	N/A	9	27	No	95±132	−29±143
20/03/2014	−566.84	−123.5	03:42:00	03:42:23	M1.7	12014	9	201	No	473±328	−350±997
21/03/2014	−590.41	382.09	10:10:00	10:21:23	C2.7	12013	12	166	Yes	65±41	−17±37
23/03/2014	−526.32	−121.24	03:00:00	02:59:23	C5.0	12014	6	146	No	376±550	−499±626
28/03/2014	339.34	286.19	19:10:00	19:11:11	M2.0	12017	30	339	Yes	655±18	−270±27
28/03/2014	369.94	284.58	23:43:00	23:45:47	M2.6	N/A	10	345	No	330±43	−117±48
29/03/2014	−541.79	366.92	01:54:00	01:59:11	C2.5	12017	16	33	Yes	308±30	−82±25
29/03/2014	501.45	275.93	17:42:00	17:44:23	X1.0	12017	20	336	Yes	530±32	−174±33
30/03/2014	650.59	213.77	11:48:00	11:48:23	N/A	12017	20	349	Yes	489±10	−233±19
01/04/2014	178.46	−127.54	18:42:00	18:43:47	C1.2	N/A	2	312	No	180±272	−78±151
02/04/2014	−745.31	294.49	13:08:00	13:15:11	M6.5	12030	10	7	No	171±66	−101±46
04/04/2014	−411.15	308.48	13:34:00	13:43:11	C8.3	12021	15	303	Yes	427±35	−167±30

Table 1 (*Continued.*)

Date	Flare X arcsec	Flare Y arcsec	t_{flare} UT	t_{wave} UT	Flare class	Active Region	Num. arcs	Central arc	Wave	Median initial vel.	Median acc.
11/04/2014	−907.12	−286.15	11:18:00	11:19:59	C9.4	N/A	8	216	No	187 ± 724	−234 ± 1611
16/04/2014	−145.69	−143.24	19:54:00	20:00:47	M1.0	12035	6	103	No	293 ± 213	−151 ± 968
18/04/2014	525.82	−209.11	12:37:00	12:39:11	M7.3	N/A	23	188	Yes	492 ± 558	−356 ± 619
19/04/2014	926.2	194.91	19:25:00	19:27:11	C4.7	N/A	3	290	No	272 ± 83	−79 ± 87
21/04/2014	161.49	312.7	03:22:00	03:25:59	N/A	N/A	3	189	No	93 ± 1452	−87 ± 1553
21/04/2014	160.75	327.98	11:05:00	11:08:11	N/A	N/A	4	79	No	40 ± 358	−18 ± 376
21/04/2014	227.61	−101.63	19:30:00	19:35:23	C5.1	12035	7	357	No	169 ± 129	−98 ± 257
29/04/2014	−242.11	−130.54	22:28:00	22:33:23	B9.0	12047	9	355	No	157 ± 86	−177 ± 93
02/05/2014	−179.01	246.99	09:17:00	09:17:23	C4.4	12047	4	132	No	302 ± 609	−231 ± 1800
08/05/2014	163.23	−109.71	03:05:00	03:06:23	N/A	N/A	4	82	No	142 ± 1872	−74 ± 3689
09/05/2014	195.39	−111.74	02:15:00	02:16:35	N/A	N/A	4	4	No	213 ± 311	−174 ± 932
12/05/2014	−495.23	−365.28	10:40:00	10:41:23	N/A	N/A	26	146	Yes	168 ± 90	−64 ± 97
15/05/2014	−148.67	−378.93	20:15:00	20:16:23	C1.0	N/A	4	196	No	160 ± 12	−61 ± 105
10/06/2014	−895.08	−277.33	12:36:00	12:40:47	X1.5	N/A	7	20	No	416 ± 0	−224 ± 3
12/06/2014	728.71	−330.34	21:34:00	21:35:35	M1.0	12087	5	238	No	145 ± 114	−57 ± 61
08/07/2014	−766.9	163.13	16:06:00	16:14:23	M6.5	12113	26	34	Yes	558 ± 16	−179 ± 5
10/07/2014	−395.4	90.25	21:01:00	21:07:11	C7.4	N/A	30	281	Yes	222 ± 12	−111 ± 11
10/07/2014	892.82	213.91	22:29:00	22:28:59	M1.5	N/A	4	293	No	167 ± 57	−144 ± 46
25/07/2014	−536.86	77.66	06:57:00	06:57:35	C2.2	12121	5	352	No	545 ± 0	−316 ± 20
01/08/2014	−16.2	102.59	10:38:00	10:43:35	C4.8	12132	9	41	No	211 ± 61	−110 ± 108
01/08/2014	−162.77	−241.27	17:55:00	17:56:59	M1.5	N/A	6	230	No	336 ± 65	−369 ± 396
20/08/2014	−439.98	65.03	13:45:00	13:47:35	N/A	N/A	11	51	Yes	307 ± 314	−219 ± 927
20/08/2014	−363.79	93.71	21:39:00	21:41:23	C2.1	12139	20	92	Yes	273 ± 268	−181 ± 303
21/08/2014	−256.7	88.91	08:43:00	08:45:47	B8.8	12146	3	39	No	821 ± 574	−541 ± 625
22/08/2014	−498.14	51.66	00:00:00	00:01:35	C6.6	N/A	5	58	No	394 ± 172	−469 ± 250

Table 1 (*Continued.*)

Date	Flare X arcsec	Flare Y arcsec	t_{flare} UT	t_{wave} UT	Flare class	Active Region	Num. arcs	Central arc	Wave	Median initial vel.	Median acc.
22/08/2014	−16.26	83.99	10:13:00	10:15:23	C2.2	12149	3	116	No	335 ± 690	−161 ± 338
22/08/2014	49.37	17.61	15:38:00	15:47:59	C6.2	12146	18	31	Yes	385 ± 168	−207 ± 183
23/08/2014	224.55	103.15	17:19:00	17:26:38	C6.0	12149	20	46	Yes	372 ± 299	−237 ± 179
24/08/2014	322.62	23.63	00:08:00	00:08:35	C1.6	12146	6	96	No	607 ± 85	−656 ± 147
24/08/2014	346.22	124.2	07:30:00	07:31:47	C2.8	12146	7	53	No	304 ± 102	−174 ± 209
25/08/2014	615.11	77.3	14:13:00	14:13:35	C1.3	12146	7	292	No	254 ± 508	−157 ± 753
25/08/2014	580.53	40.39	14:51:00	14:55:35	M2.0	12146	18	165	Yes	237 ± 294	−54 ± 119
25/08/2014	666.54	49.66	20:06:00	20:07:47	M3.9	N/A	29	175	Yes	228 ± 41	−96 ± 36
26/08/2014	696.57	86.95	02:36:00	02:36:35	C4.0	12146	6	39	No	278 ± 653	−60 ± 694
27/08/2014	819.33	107.87	05:09:00	05:12:47	C1.8	12146	5	6	No	169 ± 422	−26 ± 352
28/08/2014	920.52	106.98	15:08:00	15:09:11	C1.9	N/A	5	281	No	207 ± 34	−55 ± 604
10/09/2014	−32.4	112.6	17:21:00	17:29:50	X1.6	12158	15	15	Yes	548 ± 21	−244 ± 25
15/09/2014	797.93	255.56	18:13:00	18:14:47	C2.2	12158	2	22	No	480 ± 310	−563 ± 327
18/09/2014	−889.04	40.18	08:41:00	08:40:38	N/A	N/A	3	288	No	590 ± 229	−785 ± 257
23/09/2014	−511.04	−293.94	23:05:00	23:08:38	M2.3	12173	13	183	Yes	285 ± 94	−363 ± 71
02/10/2014	907.82	−293.16	18:49:00	18:51:59	M7.3	12173	4	125	No	595 ± 55	−822 ± 87
30/10/2014	−910.94	−108.9	13:04:00	13:05:23	C6.9	N/A	2	85	No	593 ± 114	−864 ± 385
30/10/2014	−905.42	−110.12	15:06:00	15:06:47	C2.3	12201	4	231	No	164 ± 0	−150 ± 67
30/10/2014	−880.57	−114.89	22:54:00	22:56:59	C4.8	12201	3	194	No	463 ± 69	−621 ± 337
02/11/2014	−454.99	−113.79	17:00:00	17:04:11	C3.5	N/A	7	348	No	494 ± 123	−246 ± 207
03/11/2014	−363.17	−116.27	03:47:00	03:50:47	C4.2	12201	7	338	No	423 ± 4126	−461 ± 1972
03/11/2014	−267.29	−118.11	12:20:00	12:22:23	M2.2	N/A	3	6	No	543 ± 951	−486 ± 999
05/11/2014	−879.31	228.09	09:38:00	09:39:23	M7.9	12205	10	5	No	458 ± 33	−254 ± 32
05/11/2014	−853.04	257.98	19:15:00	19:20:59	M2.9	12205	4	51	No	308 ± 223	−136 ± 79
07/11/2014	−600.07	220.96	17:05:00	17:04:47	X1.6	12205	7	284	No	474 ± 44	−177 ± 31

Table 1 (*Continued.*)

Date	Flare X arcsec	Flare Y arcsec	t_{flare} UT	t_{wave} UT	Flare class	Active Region	Num. arcs	Central arc	Wave	Median initial vel.	Median acc.
11/11/2014	−239.48	248.98	11:35:00	11:44:11	C6.7	N/A	17	19	Yes	70±15	68±29
14/11/2014	748.06	305.25	14:47:00	14:49:23	C3.1	12208	9	105	No	93±1047	−28±777
29/11/2014	−512.67	−349	01:23:00	01:29:23	C4.2	12219	8	47	No	224±17	−56±17
02/12/2014	603.07	−278.36	07:58:00	08:11:35	C5.2	12217	10	283	No	789±380	−651±275
02/12/2014	535.67	−358.76	17:26:00	17:32:23	C3.9	N/A	18	173	Yes	399±222	−337±192
05/12/2014	872.46	−366.46	05:40:00	05:46:35	C2.1	12222	7	15	No	405±1253	−151±541
06/12/2014	657.87	150.74	20:58:00	21:02:11	N/A	N/A	9	279	No	333±255	−69±97
11/01/2015	298.92	220.04	22:18:00	22:18:11	N/A	N/A	4	319	No	297±0	−36±1
09/02/2015	−810.15	289.74	22:59:00	23:13:23	M2.4	12280	13	341	Yes	279±122	−124±62
07/03/2015	−870.38	−258.9	21:45:00	21:50:35	M9.2	N/A	6	9	No	212±30	−88±18
09/03/2015	−651.66	−214.93	23:31:00	23:32:59	M5.8	N/A	11	183	Yes	245±267	−143±185
10/03/2015	−601.79	−158.5	03:19:00	03:20:23	M5.1	12297	4	51	No	437±0	−103±3
11/03/2015	−332.27	−172.36	16:11:00	16:10:59	X2.2	12297	8	235	No	321±137	−378±2459
15/03/2015	379.48	−258.28	01:15:00	01:19:47	C9.1	12297	6	110	No	77±278	−23±485
04/04/2015	−341.13	−440.11	22:40:00	22:52:11	C3.8	N/A	11	226	Yes	287±43	−246±29
06/04/2015	−225.96	−133.12	18:32:00	18:39:23	C3.0	12320	5	37	No	379±867	−285±695
05/05/2015	−905.14	256.19	13:45:00	13:47:23	M1.2	12339	5	280	No	235±70	−359±385
05/05/2015	−888.05	261.25	22:05:00	22:06:35	X2.7	N/A	7	63	No	365±82	−361±105
09/05/2015	−914.49	250.27	01:12:00	01:14:59	C7.4	N/A	7	44	No	331±0	−175±6
13/05/2015	255.97	258.71	18:09:00	18:08:11	C9.2	12343	15	348	Yes	383±373	−604±535
27/05/2015	−925.91	182.41	12:15:00	12:19:23	N/A	N/A	3	334	No	276±116	−159±151
18/06/2015	−700.38	230.56	16:30:00	16:36:11	N/A	N/A	39	269	Yes	11±39	19±93
21/06/2015	−208.55	170.53	01:26:00	01:25:35	M2.0	12371	4	183	No	337±405	−122±150
22/06/2015	129.03	166.93	17:49:00	17:52:14	M6.6	12371	12	189	Yes	378±0	−382±9
25/06/2015	625.64	121.62	08:10:00	08:30:23	M7.9	12371	33	258	Yes	398±44	−215±55

Table 1 (*Continued.*)

Date	Flare X arcsec	Flare Y arcsec	t_{flare} UT	t_{wave} UT	Flare class	Active Region	Num. arcs	Central arc	Wave	Median initial vel.	Median acc.
15/08/2015	−497.41	−239.71	12:19:00	12:29:35	C1.6	12401	6	59	No	233±1440	−194±1131
20/08/2015	−645.91	−276	05:08:00	05:16:35	C3.4	12403	12	23	Yes	448±196	−685±597
21/08/2015	−417.24	−342.79	09:34:00	09:35:23	M1.4	12403	11	16	Yes	785±90	−683±164
22/08/2015	−222.46	−352.22	06:39:00	06:40:11	M1.2	12403	19	26	Yes	699±607	−408±324
26/08/2015	719.95	−221.94	19:33:00	19:36:35	C1.7	12403	9	349	No	460±321	−284±183
17/09/2015	926.09	144.13	12:47:00	12:50:11	B.9	12415	3	24	No	71±605	−53±410
20/09/2015	659.69	−429.37	17:32:00	17:36:59	M2.1	12415	12	97	Yes	159±411	−87±283
15/10/2015	704.05	−386.39	10:26:00	10:34:47	B6.2	N/A	9	36	No	221±0	−130±35
28/10/2015	633.86	141.77	05:31:00	05:32:35	C1.2	N/A	5	230	No	306±125	−383±422
01/11/2015	272.76	199.22	21:20:00	21:24:47	C6.4	12445	15	354	Yes	291±39	−223±48
02/11/2015	447.43	239.35	20:51:00	21:03:23	N/A	N/A	18	15	Yes	499±29	−294±38
04/11/2015	681.83	220.96	01:05:00	01:05:35	B9.0	N/A	8	340	No	0±0	52±77
04/11/2015	841.09	220.71	03:21:00	03:23:11	M1.9	12445	9	92	No	305±46	−198±64
04/11/2015	879.06	227.31	11:57:00	11:56:59	M2.6	12445	10	90	No	130±0	−102±64
04/11/2015	66.73	100.61	13:31:00	13:32:59	M3.7	12443	17	44	Yes	580±421	−288±219
09/11/2015	−625.59	−229.29	12:51:00	12:51:23	M3.9	12449	6	20	No	486±359	−203±231
01/12/2015	643.05	158.15	07:57:00	08:02:23	C3.6	12458	7	80	No	561±189	−397±175
04/12/2015	−879.58	149.24	16:53:00	16:57:11	N/A	N/A	9	158	No	407±82	−247±176
11/12/2015	−268.17	−95.4	16:53:00	16:58:11	C5.6	12465	6	268	No	404±633	−233±778
23/12/2015	−807.05	−352.47	00:21:00	00:31:47	M4.7	12473	5	76	No	522±178	−276±106
28/12/2015	191.37	−295.07	11:20:00	11:23:59	M1.8	N/A	9	204	No	204±174	−124±164
01/01/2016	903.29	−324.88	23:10:00	23:12:11	M2.3	N/A	12	204	Yes	164±42	−81±28
11/02/2016	166.9	277.92	20:20:00	20:20:35	C8.9	12497	11	37	Yes	587±849	−408±978
13/02/2016	544.78	309.17	20:45:00	20:47:35	C2.5	12497	12	156	Yes	411±153	−256±87
14/02/2016	688.02	326.17	19:23:00	19:22:59	M1.0	12497	3	176	No	436±74	−595±188

Table 1 (*Continued.*)

Date	Flare X arcsec	Flare Y arcsec	t_{flare} UT	t_{wave} UT	Flare class	Active Region	Num. arcs	Central arc	Wave	Median initial vel.	Median acc.
18/04/2016	826.49	239.04	00:22:00	00:22:23	M6.7	12529	12	171	Yes	155 ± 26	-18 ± 32
14/05/2016	782.69	-90.86	09:21:00	09:22:11	N/A	N/A	6	168	No	524 ± 97	-593 ± 366
14/05/2016	800.52	-92.24	11:28:00	11:31:11	N/A	N/A	6	143	No	377 ± 0	-176 ± 20
14/05/2016	817.35	-93.7	15:15:00	15:18:11	N/A	N/A	7	143	No	842 ± 126	-881 ± 494
16/05/2016	279.88	331.87	00:51:00	00:53:35	N/A	N/A	9	235	No	395 ± 60	-288 ± 35
29/05/2016	436.17	211.4	04:40:00	04:41:23	B3.4	N/A	11	200	Yes	498 ± 558	-456 ± 784
07/06/2016	-465.89	-356.74	05:58:00	06:00:11	B1.9	N/A	14	249	Yes	103 ± 1825	-95 ± 2175
19/06/2016	463.36	174.77	11:44:00	11:48:23	C1.7	N/A	16	326	Yes	355 ± 421	-352 ± 1059
20/06/2016	570.33	175.75	02:49:00	02:50:11	B9.5	N/A	11	37	Yes	457 ± 283	-541 ± 1039
07/07/2016	519.16	-322.46	07:49:00	07:49:47	C5.1	12561	8	320	No	294 ± 484	-280 ± 323
10/07/2016	-862.79	173.71	00:53:00	01:04:14	C8.6	12564	29	347	Yes	277 ± 0	-79 ± 8
17/07/2016	-436.67	-354.32	13:50:00	13:49:59	N/A	N/A	30	224	Yes	91 ± 685	101 ± 432
20/07/2016	630.22	38.84	22:03:00	22:05:47	C4.6	12567	7	259	No	414 ± 164	-243 ± 80
23/07/2016	920.73	64.63	05:08:00	05:09:23	M7.6	12567	10	34	No	165 ± 32	-39 ± 8

References

Biesecker, D.A., Myers, D.C., Thompson, B.J., Hammer, D.M., Vourlidas, A.: 2002, Solar phenomena associated with "EIT Waves". *Astrophys. J.* **569**, 1009. DOI. ADS.

Byrne, J.P., Long, D.M., Gallagher, P.T., Bloomfield, D.S., Maloney, S.A., McAteer, R.T.J., *et al.*: 2013, Improved methods for determining the kinematics of coronal mass ejections and coronal waves. *Astron. Astrophys.* **557**, A96. DOI. ADS.

Cliver, E.W., Webb, D.F., Howard, R.A.: 1999, On the origin of solar metric type II bursts. *Solar Phys.* **187**, 89. DOI. ADS.

Cliver, E.W., Laurenza, M., Storini, M., Thompson, B.J.: 2005, On the origins of solar EIT waves. *Astrophys. J.* **631**, 604. DOI. ADS.

Delaboudinière, J.-P., Artzner, G.E., Brunaud, J., Gabriel, A.H., Hochedez, J.F., Millier, F., *et al.*: 1995, EIT: Extreme-Ultraviolet Imaging Telescope for the SOHO mission. *Solar Phys.* **162**, 291. DOI. ADS.

Delannée, C., Aulanier, G.: 1999, Cme associated with transequatorial loops and a bald patch flare. *Solar Phys.* **190**, 107. DOI. ADS.

Dere, K.P., Brueckner, G.E., Howard, R.A., Koomen, M.J., Korendyke, C.M., Kreplin, R.W., *et al.*: 1997, EIT and LASCO observations of the initiation of a coronal mass ejection. *Solar Phys.* **175**, 601. DOI. ADS.

Domingo, V., Fleck, B., Poland, A.I.: 1995, The SOHO mission: an overview. *Solar Phys.* **162**, 1. DOI. ADS.

Grechnev, V.V., Uralov, A.M., Chertok, I.M., Kuzmenko, I.V., Afanasyev, A.N., Meshalkina, N.S., Kalashnikov, S.S., Kubo, Y.: 2011, Coronal shock waves, EUV waves, and their relation to CMEs. I. Reconciliation of "EIT waves", type II radio bursts, and leading edges of CMEs. *Solar Phys.* **273**, 433. DOI. ADS.

Huttunen-Heikinmaa, K., Valtonen, E., Laitinen, T.: 2005, Proton and helium release times in SEP events observed with SOHO/ERNE. *Astron. Astrophys.* **442**, 673. DOI. ADS.

Kahler, S.: 1994, Injection profiles of solar energetic particles as functions of coronal mass ejection heights. *Astrophys. J.* **428**, 837. DOI. ADS.

Kaiser, M.L., Kucera, T.A., Davila, J.M., St. Cyr, O.C., Guhathakurta, M., Christian, E.: 2008, The STEREO mission: an introduction. *Space Sci. Rev.* **136**, 5. DOI. ADS.

Kienreich, I.W., Temmer, M., Veronig, A.M.: 2009, STEREO quadrature observations of the three-dimensional structure and driver of a global coronal wave. *Astrophys. J. Lett.* **703**, L118. DOI. ADS.

Klassen, A., Aurass, H., Mann, G., Thompson, B.J.: 2000, Catalogue of the 1997 SOHO-EIT coronal transient waves and associated type II radio burst spectra. *Astron. Astrophys. Suppl.* **141**, 357. DOI. ADS.

Klein, K.-L., Krucker, S., Lointier, G., Kerdraon, A.: 2008, Open magnetic flux tubes in the corona and the transport of solar energetic particles. *Astron. Astrophys.* **486**, 589. DOI. ADS.

Kozarev, K.A., Korreck, K.E., Lobzin, V.V., Weber, M.A., Schwadron, N.A.: 2011, Off-limb Solar coronal wavefronts from SDO/AIA extreme-ultraviolet observations – implications for particle production. *Astrophys. J. Lett.* **733**, L25. DOI. ADS.

Laitinen, T., Kopp, A., Effenberger, F., Dalla, S., Marsh, M.S.: 2016, Solar energetic particle access to distant longitudes through turbulent field-line meandering. *Astron. Astrophys.* **591**, A18. DOI. ADS.

Lario, D., Kwon, R.-Y., Vourlidas, A., Raouafi, N.E., Haggerty, D.K., Ho, G.C., Anderson, B.J., Papaioannou, A., Gómez-Herrero, R., Dresing, N., Riley, P.: 2016, Longitudinal properties of a widespread solar energetic particle event on 2014 February 25: evolution of the associated CME shock. *Astrophys. J.* **819**, 72. DOI. ADS.

Lin, R.P., Anderson, K.A., Ashford, S., Carlson, C., Curtis, D., Ergun, R., Larson, D., McFadden, J., McCarthy, M., Parks, G.K., Rème, H., Bosqued, J.M., Coutelier, J., Cotin, F., D'Uston, C., Wenzel, K.-P., Sanderson, T.R., Henrion, J., Ronnet, J.C., Paschmann, G.: 1995, A three-dimensional plasma and energetic particle investigation for the wind spacecraft. *Space Sci. Rev.* **71**, 125. DOI. ADS.

Liu, W., Ofman, L.: 2014, Advances in observing various coronal EUV waves in the SDO era and their seismological applications (Invited Review). *Solar Phys.* **289**, 3233. DOI. ADS.

Liu, W., Title, A.M., Zhao, J., Ofman, L., Schrijver, C.J., Aschwanden, M.J., De Pontieu, B., Tarbell, T.D.: 2011, Direct imaging of quasi-periodic fast propagating waves of $\sim 2000 \, \text{km s}^{-1}$ in the low solar corona by the Solar Dynamics Observatory Atmospheric Imaging Assembly. *Astrophys. J. Lett.* **736**, L13. DOI. ADS.

Long, D.M., Bloomfield, D.S., Gallagher, P.T., Pérez-Suárez, D.: 2014, CorPITA: an automated algorithm for the identification and analysis of coronal "EIT waves". *Solar Phys.* **289**, 3279. DOI. ADS.

Long, D.M., Bloomfield, D.S., Chen, P.F., Downs, C., Gallagher, P.T., Kwon, R.-Y., Vanninathan, K., Veronig, A.M., Vourlidas, A., Vršnak, B., Warmuth, A., Žic, T.: 2017, Understanding the physical nature of coronal "EIT waves". *Solar Phys.* **292**, 7. DOI. ADS.

Ma, S., Raymond, J.C., Golub, L., Lin, J., Chen, H., Grigis, P., *et al.*: 2011, Observations and interpretation of a low coronal shock wave observed in the EUV by the SDO/AIA. *Astrophys. J.* **738**, 160. DOI. ADS.

Magdalenić, J., Vršnak, B., Pohjolainen, S., Temmer, M., Aurass, H., Lehtinen, N.J.: 2008, A flare-generated shock during a coronal mass ejection on 24 December 1996. *Solar Phys.* **253**, 305. DOI. ADS.

Magdalenić, J., Marqué, C., Zhukov, A.N., Vršnak, B., Veronig, A.: 2012, Flare-generated type II burst without associated coronal mass ejection. *Astrophys. J.* **746**, 152. DOI. ADS.

Mancuso, S., Raymond, J.C.: 2004, Coronal transients and metric type II radio bursts. I. Effects of geometry. *Astron. Astrophys.* **413**, 363. DOI. ADS.

Mann, G., Classen, H.-T.: 1995, Electron acceleration to high energies at quasi-parallel shock waves in the solar corona. *Astron. Astrophys.* **304**, 576. ADS.

Mann, G., Klassen, A., Aurass, H., Classen, H.-T.: 2003, Formation and development of shock waves in the solar corona and the near-Sun interplanetary space. *Astron. Astrophys.* **400**, 329. DOI. ADS.

Miteva, R., Mann, G.: 2007, The electron acceleration at shock waves in the solar corona. *Astron. Astrophys.* **474**, 617. DOI. ADS.

Miteva, R., Klein, K.-L., Kienreich, I., Temmer, M., Veronig, A., Malandraki, O.E.: 2014, Solar energetic particles and associated EIT disturbances in solar cycle 23. *Solar Phys.* **289**, 2601. DOI. ADS.

Moreton, G.E.: 1960, Hα observations of flare-initiated disturbances with velocities ∼ 1000 km/sec. *Astron. J.* **65**, 494. DOI. ADS.

Moreton, G.E., Ramsey, H.E.: 1960, Recent observations of dynamical phenomena associated with solar flares. *Publ. Astron. Soc. Pac.* **72**, 357. DOI. ADS.

Moses, D., Clette, F., Delaboudinière, J.-P., Artzner, G.E., Bougnet, M., Brunaud, J., *et al.*: 1997, EIT observations of the extreme ultraviolet Sun. *Solar Phys.* **175**, 571. DOI. ADS.

Muhr, N., Veronig, A.M., Kienreich, I.W., Vršnak, B., Temmer, M., Bein, B.M.: 2014, Statistical analysis of large-scale EUV waves observed by STEREO/EUVI. *Solar Phys.* **289**, 4563. DOI. ADS.

Nelson, G.J., Melrose, D.B.: 1985, In: McLean, D.J., Labrum, N.R. (eds.) *Type II bursts*, 333. ADS.

Nitta, N.V., Schrijver, C.J., Title, A.M., Liu, W.: 2013, Large-scale coronal propagating fronts in solar eruptions as observed by the atmospheric imaging assembly on board the solar dynamics observatory – an ensemble study. *Astrophys. J.* **776**, 58. DOI. ADS.

Nitta, N.V., Liu, W., Gopalswamy, N., Yashiro, S.: 2014, The relation between large-scale coronal propagating fronts and type II radio bursts. *Solar Phys.* **289**, 4589. DOI. ADS.

Park, J., Innes, D.E., Bucik, R., Moon, Y.-J.: 2013, The source regions of solar energetic particles detected by widely separated spacecraft. *Astrophys. J.* **779**, 184. DOI. ADS.

Park, J., Innes, D.E., Bucik, R., Moon, Y.-J., Kahler, S.W.: 2015, Study of solar energetic particle associations with coronal extreme-ultraviolet waves. *Astrophys. J.* **808**, 3. DOI. ADS.

Patsourakos, S., Vourlidas, A.: 2009, "Extreme Ultraviolet Waves" are waves: first quadrature observations of an extreme ultraviolet wave from STEREO. *Astrophys. J. Lett.* **700**, L182. DOI. ADS.

Patsourakos, S., Vourlidas, A., Stenborg, G.: 2010, The genesis of an impulsive coronal mass ejection observed at ultra-high cadence by AIA on SDO. *Astrophys. J. Lett.* **724**, L188. DOI. ADS.

Payne-Scott, R., Yabsley, D.E., Bolton, J.G.: 1947, Relative times of arrival of bursts of solar noise on different radio frequencies. *Nature* **160**, 256. DOI. ADS.

Pesnell, W.D., Thompson, B.J., Chamberlin, P.C.: 2012, The Solar Dynamics Observatory (SDO). *Solar Phys.* **275**, 3. DOI. ADS.

Pohjolainen, S., Hori, K., Sakurai, T.: 2008, Radio bursts associated with flare and ejecta in the 13 July 2004 event. *Solar Phys.* **253**, 291. DOI. ADS.

Prise, A.J., Harra, L.K., Matthews, S.A., Long, D.M., Aylward, A.D.: 2014, An investigation of the CME of 3 November 2011 and its associated widespread solar energetic particle event. *Solar Phys.* **289**, 1731. DOI. ADS.

Reames, D.V.: 1993, Non-thermal particles in the interplanetary medium. *Adv. Space Res.* **13**, 331. DOI. ADS.

Reames, D.V.: 2009, Solar release times of energetic particles in ground-level events. *Astrophys. J.* **693**, 812. DOI. ADS.

Rouillard, A.P., Sheeley, N.R., Tylka, A., Vourlidas, A., Ng, C.K., Rakowski, C., Cohen, C.M.S., Mewaldt, R.A., Mason, G.M., Reames, D., Savani, N.P., StCyr, O.C., Szabo, A.: 2012, The longitudinal properties of a solar energetic particle event investigated using modern solar imaging. *Astrophys. J.* **752**, 44. DOI. ADS.

Thompson, B.J., Myers, D.C.: 2009, A catalog of coronal "EIT Wave" transients. *Astrophys. J. Suppl.* **183**, 225. DOI. ADS.

Thompson, B.J., Plunkett, S.P., Gurman, J.B., Newmark, J.S., St. Cyr, O.C., Michels, D.J.: 1998, SOHO/EIT observations of an Earth-directed coronal mass ejection on May 12, 1997. *Geophys. Res. Lett.* **25**, 2465. DOI. ADS.

Uchida, Y.: 1968, Propagation of hydromagnetic disturbances in the solar corona and Moreton's wave phenomenon. *Solar Phys.* **4**, 30. DOI. ADS.

Vršnak, B., Lulić, S.: 2000, Formation of coronal Mhd shock waves – I. The basic mechanism. *Solar Phys.* **196**, 157. DOI. ADS.

Vršnak, B., Warmuth, A., Temmer, M., Veronig, A., Magdalenić, J., Hillaris, A., Karlický, M.: 2006, Multi-wavelength study of coronal waves associated with the CME-flare event of 3 November 2003. *Astron. Astrophys.* **448**, 739. DOI. ADS.

Warmuth, A.: 2010, Large-scale waves in the solar corona: the continuing debate. *Adv. Space Res.* **45**, 527. DOI. ADS.

Warmuth, A.: 2015, Large-scale globally propagating coronal waves. *Living Rev. Solar Phys.* **12**, 3. DOI. ADS.

Warmuth, A., Mann, G.: 2011, Kinematical evidence for physically different classes of large-scale coronal EUV waves. *Astron. Astrophys.* **532**, A151. DOI. ADS.

Warmuth, A., Vršnak, B., Magdalenić, J., Hanslmeier, A., Otruba, W.: 2004, A multiwavelength study of solar flare waves. II. Perturbation characteristics and physical interpretation. *Astron. Astrophys.* **418**, 1117. DOI. ADS.

Wild, J.P., McCready, L.L.: 1950, Observations of the spectrum of high-intensity solar radiation at metre wavelengths. I. The apparatus and spectral types of solar burst observed. *Aust. J. Sci. Res., Ser. A* **3**, 387. DOI. ADS.

Wuelser, J.-P., Lemen, J.R., Tarbell, T.D., Wolfson, C.J., Cannon, J.C., Carpenter, B.A., *et al.*: 2004, EUVI: the STEREO-SECCHI extreme ultraviolet imager. In: Fineschi, S., Gummin, M.A. (eds.) *Telescopes and Instrumentation for Solar Astrophysics*, *Society of Photo-Optical Instrumentation Engineers (SPIE) Conference Series* **5171**, 111. DOI. ADS.

Zucca, P., Carley, E.P., Bloomfield, D.S., Gallagher, P.T.: 2014, The formation heights of coronal shocks from 2D density and Alfvén speed maps. *Astron. Astrophys.* **564**, A47. DOI. ADS.